mFas-PA system was engineered in TNFR1$^{-/-}$R2$^{-/-}$ preadipocytes, we were able to analyze hTNF-mediated hTNFR2 activity without affecting TNFR1-related apoptosis. Moreover, not only tmTNF- but also soluble TNF-mediated hTNFR2 activity was detectable using the hTNFR2/mFas-PA cell system.

In our system, hTNFR2-mediated cytotoxic activity on hTNFR2/mFas-PA cells was quantitatively determined using the WST-8 assay. Alternative methods, such as the MTT assay or Methylene Blue assay, are also capable of detecting cytotoxicity. Using the WST-8 assay, hTNFR2-mediated cytotoxic activity was readily detected 24 h after hTNF treatment (Fig. 4A), although a stronger signal was generated with a longer incubation time (48 h; Fig. 4B). Therefore, 48 h-treatment might be more appropriate for evaluating the activity of a low dose of hTNF or when analyzing an activity-weakened mutant TNF. Furthermore, if you evaluate in the absence of CHX, it may be desirable to alter the cell numbers from 1.5 to 1.0×10^4 cells/well. Previously, a similar assay system to the one described in this report was developed by Heidenreich et al. based on murine TNFR1$^{-/-}$R2$^{-/-}$ cells, which heterogenetically expressed human Fas conjugated with hTNFR2 (termed MF-R2-Fas cells) (Krippner-Heidenreich et al., 2002). However, there are some important differences between the MF-R2-Fas cells and the cell line used in our assay system (hTNFR2/mFas-PA), such as detachability. Surprisingly, unlike MF-R2-Fas cells, hTNFR2/mFas-PA cells can detect tmTNF-mediated activity as well as soluble TNF activity. Currently, the reason for this difference is unclear, although it may be caused by heterogeneity of the Fas domain. Indeed, the genetic homology between murine Fas and human Fas in IC domain is approximately 50%. Additionally, other factors may account for the observed differences between the two assay systems, such as expression level of the chimeric receptor. At any event, our results suggest that hTNFR2/mFas-PA cells will be useful in providing the basis for a highly sensitive assay system for analyzing hTNFR2 activity mediated by both soluble TNF and tmTNF. We are currently attempting to generate a TNFR2-selective mutant TNF using this assay system and a phage display system for TNF-therapy or anti-TNF therapy (unpublished data). We chose to use hTNFR2/mFas-PA cells in the screening process for a TNFR2-selective mutant TNF because this cell line is sensitive against not only purified TNF but also culture supernatants of TNF-transfected *E. coli* (crude samples). Therefore, our simple and sensitive bioassay enables high-throughput screening for TNFR2-selective mutant TNFs. The TNFR2-selective mutant will make it possible to perform a structure-function study of TNF/TNFR at any stage of function.

With the success of the human genome project, the focus of life science research has shifted to functional and structural analyses of proteins, such as disease proteomics (Oh et al., 2004; Gilchrist et al., 2006). Thus, there is increasing expectation on drug discovery/development based on the information from genomics or proteomics research, structural biology studies, or receptor-ligand interaction analyses. In particular, the therapeutic application of bioactive proteins, such as cytokines and the newly identified ligand proteins, is eagerly awaited (Gollob et al., 2003; Ansell et al., 2006). Surprisingly, however, these ligand proteins display multiple functions, which has severely limited their clinical application (Margolin et al., 1994; Eskander et al., 1997). Because the reason behind this limitation is that these ligand proteins stimulate different signal transduction pathways via multiple (two or more) receptors, the discovery of receptor-specific agonistic or antagonistic drugs is keenly awaited. Our assay system using a chimeric receptor strategy is applicable to other cytokines and thereby provides a new avenue for identifying receptor-specific agonists or antagonists. We fully anticipate that our novel technology will accelerate the development of TNFR2-related therapeutic molecules as well as acting as a research tool for studying the biology of TNFR2.

Acknowledgements

This study was supported in part by Grants-in-Aid for Scientific Research (No. 18015055, 17689008) from the Ministry of Education, Culture, Sports, Science and Technology of Japan, in part by Health Labor Sciences Research Grant from the Ministry of Health, Labor and Welfare of Japan, in part by Health Sciences Research Grants for Research on Health Sciences focusing on Drug Innovation from the Japan Health Sciences Foundation, and in part by JSPS Research Fellowships for Young Scientists from the Japan Society for the Promotion of Science.

References

Aggarwal, B.B., 2003. Signalling pathways of the TNF superfamily: a double-edged sword. Nat. Rev. Immunol. 3, 745.

Algeciras-Schimnich, A., Shen, L., Barnhart, B.C., Murmann, A.E., Burkhardt, J.K., Peter, M.E., 2002. Molecular ordering of the initial signaling events of CD95. Mol. Cell Biol. 22, 207.

Ansell, S.M., Geyer, S.M., Maurer, M.J., Kurtin, P.J., Micallef, I.N., Stella, P., Etzell, P., Novak, A.J., Erlichman, C., Witzig, T.E., 2006. Randomized phase II study of interleukin-12 in combination with rituximab in previously treated non-Hodgkin's lymphoma patients. Clin. Cancer Res. 12, 6056.

Ashkenazi, A., Dixit, V.M., 1998. Death receptors: signaling and modulation. Science 281, 1305.

Brown, S.L., Greene, M.H., Gershon, S.K., Edwards, E.T., Braun, M.M., 2002. Tumor necrosis factor antagonist therapy and lymphoma development: twenty-six cases reported to the Food and Drug Administration. Arthritis Rheum. 46, 3151.

Curtis, J.R., Patkar, N., Xie, A., Martin, C., Allison, J.J., Saag, M., Shatin, D., Saag, K.G., 2007. Risk of serious bacterial infections among rheumatoid arthritis patients exposed to tumor necrosis factor alpha antagonists. Arthritis Rheum. 56, 1125.

Dempsey, P.W., Doyle, S.E., He, J.Q., Cheng, G., 2003. The signaling adaptors and pathways activated by TNF superfamily. Cytokine Growth Factor Rev. 14, 193.

Devin, A., Cook, A., Lin, Y., Rodriguez, Y., Kelliher, M., Liu, Z., 2000. The distinct roles of TRAF2 and RIP in IKK activation by TNF-R1: TRAF2 recruits IKK to TNF-R1 while RIP mediates IKK activation. Immunity 12, 419.

Eskander, E.D., Harvey, H.A., Givant, E., Lipton, A., 1997. Phase I study combining tumor necrosis factor with interferon-alpha and interleukin-2. Am. J. Clin. Oncol. 20, 511.

Feldmann, M., Maini, R.N., 2003. Lasker Clinical Medical Research Award. TNF defined as a therapeutic target for rheumatoid arthritis and other autoimmune diseases. Nat. Med. 9, 1245.

Gilchrist, A., Au, C.E., Hiding, J., Bell, A.W., Fernandez-Rodriguez, J., Lesimple, S., Nagaya, H., Roy, L., Gosline, S.J., Hallett, M., Paiement, J., Kearney, R.E., Nilsson, T., Bergeron, J.J., 2006. Quantitative proteomics analysis of the secretory pathway. Cell 127, 1265.

Gollob, J.A., Veenstra, K.G., Parker, R.A., Mier, J.W., McDermott, D.F., Clancy, D., Tutin, L., Koon, H., Atkins, M.B., 2003. Phase I trial of concurrent twice-weekly recombinant human interleukin-12 plus low-dose IL-2 in patients with melanoma or renal cell carcinoma. J. Clin. Oncol. 21, 2564.

Heller, R.A., Song, K., Fan, N., Chang, D.J., 1992. The p70 tumor necrosis factor receptor mediates cytotoxicity. Cell 70, 47.

Jacobs, M., Togbe, D., Fremond, C., Samarina, A., Allie, N., Botha, T., Carlos, D., Parida, S.K., Grivennikov, S., Nedospasov, S., Monteiro, A., Le Bert, M.,

Quesniaux, V., Ryffel, B., 2007. Tumor necrosis factor is critical to control tuberculosis infection. Microbes Infect. 9, 623.
Katayama, K., Wada, K., Miyoshi, H., Ohashi, K., Tachibana, M., Furuki, R., Mizuguchi, H., Hayakawa, T., Nakajima, A., Kadowaki, T., Tsutsumi, Y., Nakagawa, S., Kamisaki, Y., Mayumi, T., 2004. RNA interfering approach for clarifying the PPARgamma pathway using lentiviral vector expressing short hairpin RNA. FEBS Lett. 560, 178.
Krippner-Heidenreich, A., Tubing, F., Bryde, S., Willi, S., Zimmermann, G., Scheurich, P., 2002. Control of receptor-induced signaling complex formation by the kinetics of ligand/receptor interaction. J. Biol. Chem. 277, 44155.
Margolin, K., Aronson, F.R., Sznol, M., Atkins, M.B., Gucalp, R., Fisher, R.I., Sunderland, M., Doroshow, J.H., Ernest, M.L., Mier, J.W., et al., 1994. Phase II studies of recombinant human interleukin-4 in advanced renal cancer and malignant melanoma. J. Immunother. Emphas. Immunol. 15, 147.
Micheau, O., Tschopp, J., 2003. Induction of TNF receptor I-mediated apoptosis via two sequential signaling complexes. Cell 114, 181.
Miyoshi, H., Smith, K.A., Mosier, D.E., Verma, I.M., Torbett, B.E., 1999. Transduction of human CD34+ cells that mediate long-term engraftment of NOD/SCID mice by HIV vectors. Science 283, 682.
Nathan, D.M., Angus, P.W., Gibson, P.R., 2006. Hepatitis B and C virus infections and anti-tumor necrosis factor-alpha therapy: guidelines for clinical approach. J. Gastroenterol. Hepatol. 21, 1366.
Oh, P., Li, Y., Yu, J., Durr, E., Krasinska, K.M., Carver, L.A., Testa, J.E., Schnitzer, J.E., 2004. Subtractive proteomic mapping of the endothelial surface in lung and solid tumours for tissue-specific therapy. Nature 429, 629.
Schneeweiss, S., Setoguchi, S., Weinblatt, M.E., Katz, J.N., Avorn, J., Sax, P.E., Levin, R., Solomon, D.H., 2007. Anti-tumor necrosis factor alpha therapy and the risk of serious bacterial infections in elderly patients with rheumatoid arthritis. Arthritis Rheum. 56, 1754.
Shibata, H., Yoshioka, Y., Ikemizu, S., Kobayashi, K., Yamamoto, Y., Mukai, Y., Okamoto, T., Taniai, M., Kawamura, M., Abe, Y., Nakagawa, S., Hayakawa, T., Nagata, S., Yamagata, Y., Mayumi, T., Kamada, H., Tsutsumi, Y., 2004. Functionalization of tumor necrosis factor-alpha using phage display technique and PEGylation improves its antitumor therapeutic window. Clin. Cancer Res. 10, 8293.
Shibata, H., Yoshioka, Y., Ohkawa, A., Minowa, K., Mukai, Y., Abe, Y., Taniai, M., Nomura, T., Kayamuro, H., Nabeshi, H., Sugita, T., Imai, S., Nagano, K., Yoshikawa, T., Fujita, T., Nakagawa, S., Yamamoto, A., Ohta, T., Hayakawa, T., Mayumi, T., Vandenabeele, P., Aggarwal, B.B., Nakamura, T., Yamagata, Y., Tsunoda, S., Kamada, H., Tsutsumi, Y., 2008. Creation and X-ray structure analysis of the tumor necrosis factor receptor-1-selective mutant of a tumor necrosis factor-alpha antagonist. J. Biol. Chem. 283, 998.
Stanger, B.Z., Leder, P., Lee, T.H., Kim, E., Seed, B., 1995. RIP: a novel protein containing a death domain that interacts with Fas/APO-1 (CD95) in yeast and causes cell death. Cell 81, 513.
Szlosarek, P.W., Balkwill, F.R., 2003. Tumour necrosis factor alpha: a potential target for the therapy of solid tumours. Lancet Oncol. 4, 565.
Vandenabeele, P., Declercq, W., Beyaert, R., Fiers, W., 1995. Two tumour necrosis factor receptors: structure and function. Trends Cell Biol. 5, 392.
Vandenabeele, P., Declercq, W., Vercammen, D., Van de Craen, M., Grooten, J., Loetscher, H., Brockhaus, M., Lesslauer, W., Fiers, W., 1992. Functional characterization of the human tumor necrosis factor receptor p75 in a transfected rat/mouse T cell hybridoma. J. Exp. Med. 176, 1015.
Wajant, H., Pfizenmaier, K., Scheurich, P., 2003. Tumor necrosis factor signaling. Cell Death Differ. 10, 45.
Weiss, T., Grell, M., Siemienski, K., Muhlenbeck, F., Durkop, H., Pfizenmaier, K., Scheurich, P., Wajant, H., 1998. TNFR80-dependent enhancement of TNFR60-induced cell death is mediated by TNFR-associated factor 2 and is specific for TNFR60. J. Immunol. 161, 3136.
Xu, H., Sethi, J.K., Hotamisligil, G.S., 1999. Transmembrane tumor necrosis factor (TNF)-alpha inhibits adipocyte differentiation by selectively activating TNF receptor 1. J. Biol. Chem. 274, 26287.
Yamamoto, Y., Tsutsumi, Y., Yoshioka, Y., Nishibata, T., Kobayashi, K., Okamoto, T., Mukai, Y., Shimizu, T., Nakagawa, S., Nagata, S., Mayumi, T., 2003. Site-specific PEGylation of a lysine-deficient TNF-alpha with full bioactivity. Nat. Biotechnol. 21, 546.

doi:10.1016/j.jmb.2008.11.053 J. Mol. Biol. (2009) 385, 1221–1229

JMB

Available online at www.sciencedirect.com

ScienceDirect

ELSEVIER

Structure–Function Relationship of Tumor Necrosis Factor (TNF) and Its Receptor Interaction Based on 3D Structural Analysis of a Fully Active TNFR1-Selective TNF Mutant

Yohei Mukai[1,2], Hiroko Shibata[2], Teruya Nakamura[3], Yasuo Yoshioka[2,4], Yasuhiro Abe[2], Tetsuya Nomura[1,2], Madoka Taniai[5], Tsunetaka Ohta[5], Shinji Ikemizu[3], Shinsaku Nakagawa[1], Shin-ichi Tsunoda[2], Haruhiko Kamada[2], Yuriko Yamagata[3] and Yasuo Tsutsumi[1,2]*

[1]*Graduate School of Pharmaceutical Sciences, Osaka University, 1-6 Yamadaoka, Suita, Osaka 565-0871, Japan*

[2]*Laboratory of Pharmaceutical Proteomics, National Institute of Biomedical Innovation, Osaka 567-0085, Japan*

[3]*Graduate School of Pharmaceutical Sciences, Kumamoto University, Kumamoto 862-0973, Japan*

[4]*The Center for Advanced Research and Education in Drug Discovery and Development, Osaka University, 1-6 Yamadaoka, Suita, Osaka 565-0871, Japan*

[5]*Hayashibara Biochemical Laboratories, Inc., 1-2-3 Shimoishii, Okayama 702-8006, Japan*

Received 9 July 2008; received in revised form 21 November 2008; accepted 22 November 2008
Available online 6 December 2008

Edited by I. Wilson

Tumor necrosis factor (TNF) is an important cytokine that suppresses carcinogenesis and excludes infectious pathogens to maintain homeostasis. TNF activates its two receptors [TNF receptor (TNFR) 1 and TNFR2], but the contribution of each receptor to various host defense functions and immunologic surveillance is not yet clear. Here, we used phage display techniques to generate receptor-selective TNF mutants that activate only one TNFR. These TNF mutants will be useful in the functional analysis of TNFR.

Six amino acids in the receptor binding interface (near TNF residues 30, 80, and 140) were randomly mutated by polymerase chain reaction. Two phage libraries comprising over 5 million TNF mutants were constructed. By selecting the mutants without affinity for TNFR1 or TNFR2, we successfully isolated 4 TNFR2-selective candidates and 16 TNFR1-selective candidates, respectively. The TNFR1-selective candidates were highly mutated near residue 30, whereas TNFR2-selective candidates were highly mutated near residue 140, although both had conserved sequences near residues 140 and 30, respectively. This finding suggested that the phage display technique was suitable for identifying important regions for the TNF interaction with TNFR1 and TNFR2. Purified clone R1-6, a TNFR1-selective candidate, remained fully bioactive and had full affinity for TNFR1 without activating TNFR2, indicating the usefulness of the R1-6 TNF mutant in analyzing TNFR1 receptor function.

To further elucidate the receptor selectivity of R1-6, we examined the structure of R1-6 by X-ray crystallography. The results suggested that R31A and R32G mutations strongly influenced electrostatic interaction with TNFR2, and that L29K mutation contributed to the binding of R1-6 to TNFR1. This phage display technique can be used to efficiently construct functional mutants for analysis of the TNF structure–function relationship, which might facilitate *in silico* drug design based on receptor selectivity.

Keywords: TNF; X-ray crystallography; phage display system; TNF mutant; receptor specificity

*Corresponding author. Department of Toxicology, Graduate School of Pharmaceutical Sciences, Osaka University, 1-6 Yamadaoka, Suita, Osaka 565-0871, Japan. E-mail address: ytsutsumi@phs.osaka-u.ac.jp.

Abbreviations used: TNF, tumor necrosis factor; TNFR, TNF receptor; SPR, surface plasmon resonance; wtTNF, wild-type TNF; PDB, Protein Data Bank.

Introduction

Tumor necrosis factor (TNF) is as an important immunity-modulating cytokine that is required for human body defense against infectious diseases and carcinogenesis.[1] Excess TNF, however, causes various autoimmune diseases, such as rheumatoid arthritis, Crohn's disease, and ulcerative colitis.[2–4] The relationship between TNF and disease deterioration must be unraveled before effective therapies can be developed. Both TNF receptor (TNFR) types TNFR1 and TNFR2, which induce different cell signaling, must be analyzed to better understand the function of TNF. Experiments with TNFR knockout mice have revealed the individual functions of TNFR1 and TNFR2 against viral infection, microbial pathogens, and tumor immunity.[5–8] The lack of one TNFR type, however, can affect the function of the other receptor type and weaken its signaling because the two receptors work together by crosstalk signaling.[9–11] This issue complicates investigations of the individual roles of TNFR1 and TNFR2, and the analysis of TNFR function. Therefore, many researchers have attempted to activate only one receptor using a receptor-selective TNF mutant that does not impair the function of the receptor.

In the past decade, several receptor-selective TNF mutants, which are useful for functional analysis of TNFRs, have been constructed.[12,13] Traditional point mutation methods, however, are labor-intensive because a large number of candidates must be individually assessed; therefore, it has been difficult to successfully isolate the desired mutants.[14–17] In particular, a receptor-selective TNF mutant with full bioactivity was difficult to develop due to the fact that a region on TNF shares a binding affinity for the two different receptors.[18,19] Furthermore, inadequate mutations cause a loss of affinity for both TNFR1 and TNFR2, which has made it difficult to create novel mutants with high selectivity and full bioactivity.[20] Therefore, functional analysis of TNFR using these mutants has not progressed sufficiently.

We previously developed a modified phage display technique that can be used to create desired functional mutant proteins. Using this technique, we have successfully created many mutants with high bioactivity,[21] high *in vivo* stability,[22] and antagonist activity[23] that are suitable for drug development. The advantage of this method is that it allows us to obtain information about specific functions and associated sequences, which is very useful for determining the structure–function relationship of a specific protein. This information will be useful for improving the design of therapeutic mutants.

In the present study, we used the phage display technique to create novel receptor-selective TNF mutants with full bioactivity. Structural information of the mutants was determined by crystallographic analysis, and structural simulation was used to determine a feasible basis for receptor selectivity. These TNF mutants will be useful tools for analyzing TNFR signaling. An understanding of the structure and sequence of these functional mutants, combined with bioinformatics techniques, can potentially lead to the design of a desired functional protein, peptide, or peptide mimic, and thus accelerate the development of novel strategies for analyzing disease-related proteins, such as TNF, and the development of associated therapies.

Results

Library construction and selection of receptor-selective TNF mutants

To create receptor-specific TNF mutants using our phage display system, we prepared two phage libraries, Libraries I and II. Each library contained six amino acids randomized in a receptor binding site suggested by point mutation analysis and X-ray crystallography (Fig. 1).[16,17,24] For construction of the TNF mutant library, a mutant TNF-Lys(−) gene was used as template for polymerase chain reaction (PCR) mutagenesis.[22] Sequence analysis of randomly selected clones indicated that Libraries I and II contained 8.2×10^6 and 5.6×10^6 independent clones, respectively. For selection from the library, several rounds of affinity panning were performed against human TNFR1 or TNFR2 using BIAcore 3000. Potent binders to TNFR1 or TNFR2 were concentrated in the library through this panning procedure. The monoclonal candidates in each library were picked up for enzyme-linked immunosorbent assay (ELISA) screening to confirm their receptor binding specifi-

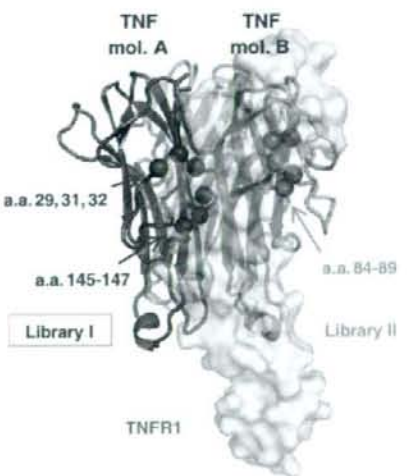

Fig. 1. Positions of randomized residues on the binding interface of the TNF–TNFR1 complex. Mutational residues of Library I (red spheres) and Library II (orange spheres). Green cartoon represents wtTNF. White area represents the surface of the TNFR1 monomer. This binding model structure of the TNF–TNFR1 complex was constructed based on the crystal structure of the LTα–TNFR1 complex (1TNR) and that of wtTNF (1TNF).

Table 1. Substituted residues of TNF mutants from Libraries I and II

			29	31	32	84	85	86	87	88	89	145	146	147
		wtTNF	L	R	R	A	V	S	Y	Q	T	A	E	S
		mutTNF-Lys(−)	—	—	—	—	—	—	—	—	—	—	—	—
TNFR1-selective candidates	Library I (29:32–145:147)	R1-1	I	—	—	—	—	—	—	—	—	—	—	—
		R1-2	Q	—	W	—	—	—	—	—	—	—	—	—
		R1-3	T	G	Y	—	—	—	—	—	—	—	—	—
		R1-4	T	K	Y	—	—	—	—	—	—	—	—	—
		R1-5	T	—	F	—	—	—	—	—	—	—	T	—
		R1-6	K	A	G	—	—	—	—	—	—	—	S	T
	Library II (84:89)	R1-7	—	—	—	S	K	T	—	T	H	—	—	—
		R1-8	—	—	—	S	P	L	—	P	K	—	—	—
		R1-9	—	—	—	S	T	N	—	N	G	—	—	—
		R1-10	—	—	—	T	S	A	—	G	P	—	—	—
		R1-11	—	—	—	T	T	A	—	S	G	—	—	—
		R1-12	—	—	—	T	H	K	—	P	Q	—	—	—
		R1-13	—	—	—	S	K	T	—	S	H	—	—	—
		R1-14	—	—	—	S	S	H	—	R	F	—	—	—
TNFR2-selective candidates	Library I (29:32–145:147)	R2-1	—	—	—	—	—	—	—	—	—	K	D	T
		R2-2	—	—	—	—	—	—	—	—	—	R	T	D
		R2-3	—	—	—	—	—	—	—	—	—	R	E	T
		R2-4	—	—	—	—	—	—	—	—	—	A	D	D
		R2-5	—	—	—	—	—	—	—	—	—	A	N	D

Conserved residues compared with wtTNF are indicated by an em dash (—). Mutated residues in each library are highlighted in gray. Library I included mutated residues 29, 31, 32, and 145–147. Library II contained mutated residues 84–89. R1-1–R1-6 and R1-7–R1-14 were isolated from Libraries I and II, respectively, as TNFR1-selective candidates. TNFR2-selective clones R2-1–R2-5 were isolated from Library I; Library II contained no TNFR2-selective clones.

city. Several clones with TNFR1 or TNFR2 specificity were eventually obtained.

Sequence analysis of receptor-specific TNF mutant candidates

Sequence analysis revealed that we had 14 TNFR1-selective candidates (R1-1–R1-14) and 5 TNFR2-selective candidates (R2-1–R2-5) from Libraries I and II (Table 1). Unfortunately, Library II did not contain any TNFR2-selective mutants. All active TNFR1-selective mutants in Library II retained Tyr87, suggesting that Tyr87 was an essential residue for receptor binding. Analysis of Library I, however, revealed that the mutated and conserved regions of the TNFR1-selective mutants were different from

Table 2. Receptor-selective bioactivities and affinities of TNF mutants

			Relative affinity (% K_d)[a]			Relative bioactivity (% of EC_{50})		
		TNFs	TNFR1	TNFR2	R_1/R_2	HEp2[b]	PC60[c]	R_1/R_2
		wtTNF	100	100	1.0	100	100	1.0
		mutTNF-Lys(−)	108	88	1.2	116	126	0.9
TNFR1-selective candidates	Library I (29:32–145:147)	R1-1	145	121	1.2	492	NT	—
		R1-2	212	32	6.7	436	NT	—
		R1-3	42	18	2.4	343	NT	—
		R1-4	43	3	13.4	447	NT	—
		R1-5	177	2	106.2	582	36	16.2
		R1-6	33	4	8.4	128	<0.07	>1800.0
	Library II (84:89)	R1-7	108	13	8.4	102	NT	—
		R1-8	145	9	16.5	120	173	0.7
		R1-9	175	24	7.4	110	NT	—
		R1-10	149	9	17.0	134	NT	—
		R1-11	219	11	20.4	58	NT	—
		R1-12	51	15	3.5	21	NT	—
		R1-13	51	11	4.6	26	NT	—
		R1-14	46	4	12.0	47	47	1.0
TNFR2-selective candidates	Library I (29:32–145:147)	R2-1	83	112	0.741	12.4	23	0.539
		R2-2	3	143	0.020	0.2	30	0.007
		R2-3	38	225	0.169	2.5	12	0.208
		R2-4	51	572	0.089	6.2	19	0.326
		R2-5	94	324	0.290	13.4	39	0.344

The affinity and bioactivity values are shown as relative values (% wtTNF).

NT, not tested.

[a] Affinity for immobilized TNFR1 and TNFR2 was assessed by SPR using BIAcore 3000.

[b] Human TNFR1-mediated bioactivity was evaluated using a HEp-2 cell cytotoxicity assay. In this assay, HEp-2 cell viability was determined by methylene blue staining. Each value represents the mean±SD.

[c] Human TNFR2-mediated bioactivity was evaluated using PC60-R2 assay. GM-CSF expression by TNFR2-mediated signaling was detected by ELISA. Each value presents the mean±SD.

those of the TNFR2-selective mutants. TNFR1-selective mutants were highly mutated near residue 30 and conserved near residue 140. On the other hand, TNFR2-selective mutants were mutated near residue 140 and conserved near residue 30. This interesting result suggested that the details of the essential binding interface for TNFR1 and TNFR2 differed despite their predicted similar complex forms.[19]

Receptor selectivity and bioactivity of TNF mutants

To investigate the properties of candidate receptor-selective TNF mutants in detail, we prepared recombinant protein using the previously described methods.[21,22] TNF mutants expressed as an inclusion body in *Escherichia coli* were denatured and refolded. Then, active TNF mutants were purified by ion-exchange and gel-filtration chromatography. TNF mutant purity was greater than 90% in sodium dodecyl sulfate–polyacrylamide gel electrophoresis, and all mutants were confirmed to form trimers by gel-filtration analysis (data not shown).

We examined the affinities of these recombinant TNF mutants for TNFR1 and TNFR2 (Table 2). Most of the TNFR1-selective candidates had little affinity for TNFR2 based on surface plasmon resonance (SPR) analysis by BIAcore 3000. In particular, the TNFR1 affinities of R1-2, R1-5, R1-8, R1-9, R1-10, and R1-11 were higher than that of wild-type TNF (wtTNF), despite the loss of their TNFR2 affinities. TNFR1- and TNFR2-mediated bioactivities were assessed by HEp-2 and PC60-hTNFR2 assays, respectively. Interestingly, R1-selective candidates from Library I showed more potent activity via TNFR1 than those from Library II. R1-5 and R1-6 showed superior bioactivity and receptor selectivity. R1-6 was selected as the best overall mutant with greater than 1800-fold selective TNFR1 activity. These mutants were novel because TNFR1-selective mutants with higher bioactivity had not yet been established. Similar studies were performed with the TNFR2-selective candidates. In SPR analysis, these candidates showed higher TNFR2 affinity than wtTNF. Unfortunately, however, none of the TNFR2-selective candidates could sufficiently activate TNFR2 and had less than 40% of the bioactivity of wtTNF.

Next, we performed a competitive binding assay to confirm the details of the TNFR1 selectivity of R1-5 and R1-6—the candidates with the highest selectivity for TNFR1. Competitive affinities were assessed under a certain amount of wtTNF-FLAG, wtTNF fusing FLAG-tag (DYKDDDDK) at C-terminal, as competitor (Fig. 2). Similar to the results of the SPR analysis, R1-5 showed a higher affinity for TNFR1 compared with wild type, and its affinity for TNFR2 was decreased to approximately 10% that for wtTNF, suggesting that R1-5 was a TNFR1-selective mutant. In contrast to the SPR results, however, R1-6 showed a higher competitive affinity for TNFR1, and wtTNF–FLAG binding to TNFR2 was not completely inhibited, even by excess R1-6, which suggested that R1-6

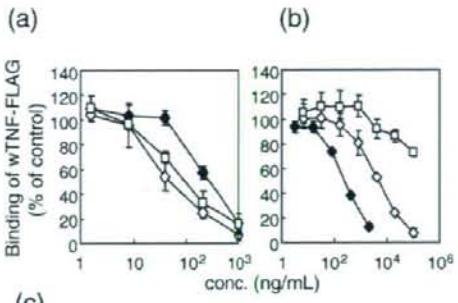

(c)

	TNFR1		TNFR2	
	IC50 (ng/ml)	(%)	IC50 (ngml)	(%)
wtTNF	276.0	100.0	508.1	100.0
R1-5	57.7	478.3	4606.6	11.0
R1-6	105.4	261.9	>100000.0	<0.5

Fig. 2. Competitive binding affinities of TNFR1-selective mutants (R1-5 and R1-6). Competitive affinities were assessed under 50 ng/ml FLAG-tagged wtTNF (wtTNF–FLAG) as competitor. Both (a) TNFR1 and (b) TNFR2 were immobilized. Binding of wtTNF–FLAG was inhibited by serially diluted TNF mutants. Final binding of wtTNF–FLAG was assessed by ELISA. Each value represents the mean±SD. (c) IC_{50} values are given as the concentration of the TNF mutant required to inhibit 50% of the maximal binding of wtTNF–FLAG.

lacked binding potency to TNFR2. Because the TNF binding interfaces to the receptors are known to overlap,[19] TNFR1 selectivity caused by a structural change in the R1-6 surface might provide important information for structure-based drug discovery.

X-ray crystallography of TNFR1-selective TNF mutant R1-6

The structural basis of the TNFR1 selectivity of R1-6 was examined by X-ray crystallography. After establishing crystallization conditions, good-quality crystals of R1-6 were obtained (approximately 0.2 mm×0.2 mm×0.3 mm in size). X-ray diffraction data were collected in SPring-8 (a large synchrotron radiation facility in Harima, Japan). Analysis of these data indicated that the space group is *R*3 and that the lattice constants are $a=135.87$ Å, $b=135.87$ Å, and $c=58.02$ Å (Table 3). The R1-6 structure was further refined using the CNS software suite. The results of model validation using the PROCHECK program indicated that there were 86.9% residues in the most favored regions, 13.1% residues in the additionally allowed regions, 0.0% residues in the generously allowed regions, and 0.0% residues in the disallowed regions.

The overall structures of the R1-6 [Protein Data Bank (PDB) code 2ZJC] and wtTNF (PDB code 1TNF) trimers are also similar and superimpose with an rmsd of 1.21 Å for 428 C^{α} atoms (Fig. 3). The structure of

Table 3. Crystallographic parameters and refinement statistics of the R1-6 crystal

Data collection	
Resolution (Å)	50–2.50 (2.59–2.50)
Cell constants (Å)[a]	135.9, 135.9, 58.0
Space group	*R*3
Measured reflections	74,516
Unique reflections	13,445 (1173)
Completeness (%)	99.9 (85.2)
R_{merge} (%)[b]	0.10 (0.53)
$I/\sigma(I)$	28.9 (4.2)
Refinement statistics	
Resolution (Å)	25.67–2.50
Reflections used	12,060
R_{cryst} (%)[c]	20.1
R_{free} (%)[d]	27.2
Completeness (%)	97.1
Atoms	
Protein; water	3338; 59
rmsd from ideality	
Bond lengths (Å); bond angles (°)	0.009; 1.27
Overall *B*-factor (Å^2)	19.7
B-factor rmsd (Å^2)	
Main-chain bonds; side-chain bonds	0.42; 0.77
Main-chain angles; side-chain angles	0.94; 1.48
Ramachandran plot statistics	
Most favored regions (%)	86.9
Additionally allowed regions (%)	13.1
Generously allowed regions (%)	0.0
Disallowed regions (%)	0.0

Values in parentheses are those for the outer shell.

[a] Cell constants are *a*, *b*, and *c*.

[b] $R_{merge} = \sum |I - \langle I \rangle| / \sum \langle I \rangle$, where I is intensity of the observations. R_{merge} in the last shell is high because of the anisotropic mosaicity of the crystal.

[c] $R_{cryst} = \sum ||F_o| - |F_c|| / \sum |F_o|$, where F_o and F_c are the observed and calculated structure factors, respectively.

[d] R_{free} is calculated as for R_{cryst}, but for the test set comprising reflections not used in refinement. The overall *B*-factor was calculated after TLS parameter analysis (TLSANL) using Refmac.

each monomer is similar to each other (rmsd of 0.98–1.12 Å for 140 C^α atoms). Especially, the structures of the β-sheet in each monomer are essentially the same (rmsd of 0.31–0.42 Å for 63 C^α atoms). These features have been found in the wtTNF trimer.[25]

The R1-6 loop structure near mutational residues 31 and 32 is different from that in wtTNF (Fig. 4). This loop structure between monomers is not different (wtTNF: rmsd of 0.61–0.72 Å for 11 C^α atoms; R1-6: rmsd of 0.39–0.91 Å for 11 C^α atoms) (Fig. 4a and b). However, they are clearly different between wtTNF and R1-6 (Fig. 4c). This structural change is thought to be caused by R32G mutation from a sterically bulky arginine residue to a flexible glycine residue. Because this region is close to the TNFR surface, such a structural change in the C^α chain could influence receptor binding. Additional TNF–TNFR docking simulation studies are discussed below.

Discussion

We recently developed the technology to create functional mutant proteins with high bioactivity, high *in vivo* stability, and antagonistic activity.[21–23] Here, we attempted to establish fully bioactive receptor-selective TNF mutants for functional analysis of TNFR1 and TNFR2 using our optimized phage display system. We constructed TNF mutant libraries (Libraries I and II) in which six residues near the receptor binding region were randomized (Fig. 1). From these libraries, we screened for TNFR1- or TNFR2-selective binders, and isolated receptor-selective candidates (Table 1). Despite the successful isolation of TNFR2-selective binders, the TNFR2-selective candidates obtained could not sufficiently activate TNFR2. This result suggested that the production of TNFR2-selective mutants was very rare in our library and that an improved panning method was necessary.

One advantage of our phage-display-based technique is that it can be used to obtain the sequence information of many mutants (Table 1). Tyr87 of TNF was conserved in all mutants obtained from Library II. This residue is highly conserved throughout the TNF superfamily, such as in LTα, LTβ, and LIGHT, and site-directed mutagenesis of the Tyr87 residue of TNF results in a dramatic loss of its biologic activity and its affinities for both TNFR1 and TNFR2.[17] In addition, Tyr87 replacement in antagonistic TNF causes unstable receptor binding and loss of receptor activation in our report.[23] These findings together indicate that Tyr87 is an essential residue for receptor signaling and receptor complex stability.

TNFR1-selective mutants had mutations near residue 30 and conserved residues near residue 140. In contrast, TNFR2-selective mutants had mutations near residue 140 and conserved residues near residue 30. These findings support those of previous point mutation analyses[15–17] and suggest that our phage-

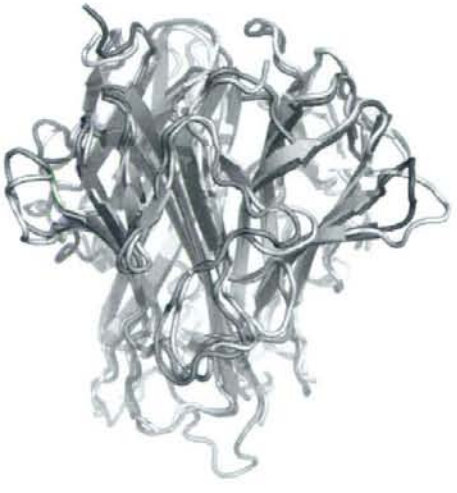

Fig. 3. Overall structure of wtTNF and R1-6. Merge image of previously reported wtTNF structure (green; 1TNF) and refined structure of R1-6 (white; 2ZJC). The flexible loop containing residues 100–110 shown at the bottom of the figure was disordered in the R1-6 structure.

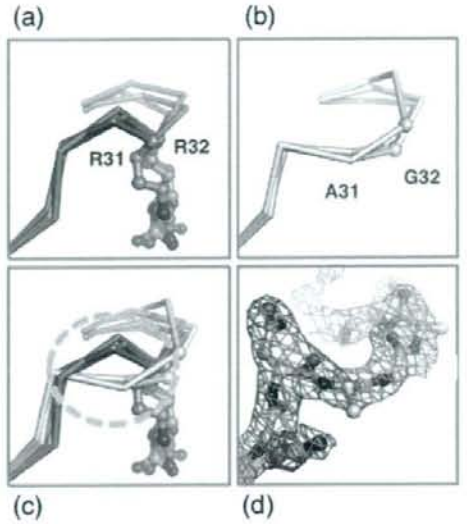

Fig. 4. Structural difference in receptor binding loop between wtTNF and R1-6. Each TNF monomer was superimposed using the CCP4i program. Details of the receptor binding loop, including residues 31 and 32, are shown in these figures. (a) Loops of wtTNF monomers (green); (b) loops of R1-6 monomers (white); (c) merged image of the loops of wtTNF and R1-6; (d) $2F_o-F_c$ map contoured at 1.0σ of R1-6 loop (pink mesh). The different C^α chains are highlighted by the dashed orange circle in (c).

display-based technique can be used to rapidly gather important information about the function–sequence relationships determined by long-term point mutation analysis. In the present study, we successfully isolated mutants that retained TNFR affinity from a huge phage library containing over a million repertoires. Most of the mutants in the library had no TNFR affinity and were therefore discarded through this selection step. This finding may indicate that the mutational residues in these unbound clones diminish TNFR affinity. This method may be useful for examining the function, capability, and sequence–function relationship of unknown cytokines and proteins.

Using these receptor-selective candidates, we expressed recombinant proteins and estimated their bioactivities and affinities for TNFR1 and TNFR2. R1-6, the most highly TNFR1-selective mutant, bound and activated TNFR1 efficiently despite the loss of its affinity for TNFR2. X-ray crystallography of R1-6 revealed that the crystal structure of R1-6 was a trimer (similar to wtTNF), and no other salient differences in the overall structure were observed. Superimposition of wtTNF and R1-6 sequences, however, revealed that the C^α of the receptor binding loop near residue 30 was partially different (Fig. 4). This change might influence the receptor binding mode of R1-6. We further used the superimposition program to perform docking simulations with TNF and TNFR1 based on the crystal structure of the LTα–TNFR1 complex (PDB code 1TNR).[18]

Based on the model wtTNF–TNFR1 complex, Arg31 of TNF would interact electrostatically with Glu56 of TNFR1. The main chain of TNF was too close to His69 of TNFR1, however, potentially causing potential steric hindrance (Fig. 5a). On the other hand, a structural change in the loop in R1-6, however, was thought to solve this problem (Fig. 5b). Arg32 of wtTNF associated with Ser72 of TNFR1 (Fig. 5a). In the R1-6 structure, however, this role of Arg32 was thought to be compensated for by Lys29 (Fig. 5b). This speculation was supported by the crystal structure of the LTα–TNFR1 complex.[18] The position of Lys29 in R1-6 corresponded to that of Arg46 in LTα interacting with Ser72 of TNFR1 by hydrogen bonding. This interesting "compensating role of an amino acid" would be difficult to induce using single point mutation methods, which is another advantage of our modified phage display technique.

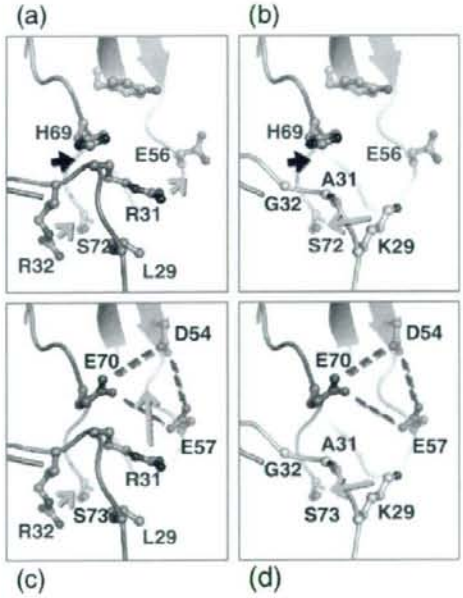

Fig. 5. Model of TNF binding to TNFR1 and TNFR2. Receptor binding interfaces of (a) wtTNF–TNFR1 (green–red); (b) R1-6–TNFR1 (white–red); (c) wtTNF–TNFR2 (green–blue); and (d) R1-6–TNFR2 (white–blue). The TNF–TNFR1 model complex was constructed from 1TNF (wtTNF) and 1TNR (LTα–TNFR1 complex). The predicted TNFR2 structure was constructed by side-chain mutation using the O program. In this simulation, the side chains of each structure were rotated to fit the predicted interaction. Stable structures of these rotamers were constructed using the O program. Steric hindrance might have occurred between His69 of TNFR1 and Arg32 of wtTNF in (a) (black arrowhead). Potential interactions are indicated by orange arrows. A cluster of anionic charged residues (Asp54, Glu57, and Glu70) is highlighted by a broken red line.

Next, we examined the TNFR1 selectivity of R1-6 based on its structure. Because the structure of TNFR2 is thought to be similar to that of TNFR1,[18] we generated a model structure of TNFR2 by manual mutation based on the crystal structure of TNFR1. This TNF–TNFR2 simulation is speculative, but this model, together with the information obtained from previous mutation studies, can be used to form hypotheses regarding the important structural features for TNFR1 selectivity. The binding surface of TNFR2 was composed of Asp54, Glu57, and Glu70, which could cause a strongly negatively charged surface of TNFR2 different from that of TNFR1 (Fig. 5c and d). Arg31 of wtTNF was thought to have an important role in TNFR2 binding by strongly interacting with this surface (Fig. 5c). R1-6 had an R31A mutation, however, which could cause the loss of the affinity of R1-6 for TNFR2 (Fig. 5d). In support of this finding, a single point mutation R31E mutant was previously reported to have a dramatic loss of affinity for TNFR2.[12,14] On the other hand, the R32W mutant is also reported to be a mutant with TNFR1 selectivity.[12] From our library, Arg32 of our TNFR1-selective candidates was replaced with hydrophobic or nonionic amino acids (Trp, Tyr, Phe, and Gly), which might indicate the importance of Arg32 for binding to TNFR2 (Table 1). This structural information, in combination with bioinformatics technology, will be useful for designing more advanced TNFR-selective mutants and TNFR-selective inhibitors (peptide mimics and chemical compounds).

In conclusion, the phage display technique is an attractive method for creating functional mutants, as demonstrated here by the production of TNFR-specific mutants. Application of this method to various cytokines and proteins will enhance the construction of useful receptor-selective mutants and accelerate functional analysis of these proteins. As an advanced application, analysis of the "structure (sequence)–function relationship" using the obtained mutants will be a powerful technique for basic life science research and drug discovery.

Materials and Methods

Cell culture

HEp-2 cells (a human fibroblast cell line) were provided by the Cell Resource Center for Biomedical Research (Tohoku University) and maintained with RPMI 1640 containing 10% fetal bovine serum and antibiotics. PC60-hTNFR2 cells (a mouse–rat fusion hybridoma comprised of human TNFR2-transfected PC60 cells) were provided by Dr. Vandenabeele and maintained in RPMI 1640 supplemented with 10% fetal bovine serum, 1 mM sodium pyruvate, 5×10^{-5} M 2-mercaptoethanol, 3 μg/ml puromycin, and antibiotics (100 U/ml penicillin, 100 μg/ml streptomycin, and 0.25 μg/ml amphotericin B).

Library construction

The pCANTAB phagemid vector (GE Healthcare Ltd., UK) encoding mutTNF-Lys(−) was used as template for PCR. This TNF was previously reported to be a fully active lysine-deficient TNF mutant.[22] Mutations were introduced in TNF at six amino acid codons (Library I: amino acid residues 29, 31, 32, and 145–147; Library II: amino acid residues 84–89) using a two-step PCR. Three primers, Oligos A, B, and C, were used for the construction of Library I. The first PCR was performed using Oligos A and B. The PCR conditions were 5 min at 95 °C, 35 cycles of denaturization at 95 °C for 15 s, and annealing/extension at 68 °C for 2 min. This first PCR product and Oligo C were then annealed to the template, and PCR was performed again under the same conditions. For the construction of Library II, Oligos A, D, and E were used. The first PCR was performed using Oligos A and D. The first PCR product and Oligo E were used as primers for the second PCR. The PCR conditions of Library II were the same as those of Library I. After the second PCR, the PCR products were digested with HindIII and NotI, and then ligated to a pY03′ phagemid vector (modified from pCANTAB) for the display of TNF variants on the phage surface as g3p fusion proteins. The primer sequences used in this experiment are listed below. Oligos A and E were designed to prime to the pCANTAB vector sequence: Oligo A: 5′-GATAACAA-TTTCACACAGGAAACAGCTATGACCATGATTACGC-CAAGCTTTGGAGCC-3′; Oligo B: 5′-CGCCATTGGCCA-GGAGGGCATTAGCSNNSNNGTTSNNCCACTGGAG-CTGCCCCTCAGCTTGAGGG-3′; Oligo C: 5′-CCAGCG-GATCCGGATACGGCACCGGCGCACCTGCGGCCGC-GGATCCACCACCACCCAGGGCAATGATCCCAAAG-TAGACCTGCCCSNNSNNSNNAAAGTCGAGATA-GTCGGGCCGATTGA-3′; Oligo D: 5′-CTGGCAGGGGC-TGCGGATGGCAGAGAGGAGATTGACGGGSNNSN-NSNNSNNSNNSNNGATGCGGCTGATGGTGTGGG-TGAGGAGCAC-3′; Oligo E: 5′-TGCGGCACGCGGTTC-CAGCGGATC-3′.

Isolation of receptor-selective TNF mutants from the library (affinity panning and screening)

Human TNFR1 Fc (R&D Systems, Inc., Minneapolis, MN) and TNFR2 Fc (R&D Systems, Inc.) were diluted to 50 μg/ml in 10 mM sodium acetate buffer (pH 4.5) and immobilized on a CM3 sensor chip using an amine coupling kit (GE Healthcare Ltd.), which resulted in an increase of 4000–6000 resonance units. The phage library (1×10^{11} colony-forming units/100 μl) was injected at 3 μl/min over the sensor chip. After binding and until the association phase had been reached, the sensor chip was washed using the rinse command and eluted using 20 μl of 10 mM glycine–HCl. The eluted phage was neutralized with 1 M Tris–HCl (pH 6.9). *E. coli* (TG1) was infected with the collected phage for amplification. This panning cycle was performed two more times. After picking up a single clone of transfected *E. coli*, the phagemid vectors were sequenced using a Big Dye Terminator v3.1 kit and ABI PRISM 3100 (Applied Biosystems Ltd., Pleasanton, CA). After the procedure, the binding affinities of the TNF mutants were assessed by ELISA, and their bioactivities through TNFR1 were determined by cytotoxicity assay in human HEp-2 cells.

Expression and purification of TNF mutants

The protocol for the expression and purification of recombinant protein was the same as that described previously.[21,22] Briefly, TNF mutants were produced in the *E. coli* BL21(DE3) strain. The inclusion body of each

TNF mutant was washed in 2.5% Triton X-100 and solubilized in 6 M guanidine–HCl, 0.1 M Tris–HCl (pH 8.0), and 2 mM ethylenediaminetetraacetic acid. Solubilized protein at 10 mg/ml was reduced with 10 mg/ml dithioerythritol for 4 h at room temperature and refolded by 100-fold dilution in a refolding buffer (100 mM Tris–HCl, 2 mM ethylenediaminetetraacetic acid, 0.5 M arginine, and 551 mg/L oxidized glutathione). After dialysis with 20 mM Tris–HCl (pH 7.4) containing 100 mM urea, active trimeric proteins were purified by ion-exchange chromatography using Q-Sepharose FF (GE Healthcare Ltd.). Size-exclusion chromatography was performed using a Superose 12 column (GE Healthcare Ltd.).

In vitro bioactivity of TNF mutants

HEp-2 cells were used for cytotoxicity assay in the presence of cycloheximide (50 μg/ml). HEp-2 cytotoxicity was dependent on TNFR1 signaling. HEp-2 cells were cultured in 96-well plates in the presence of TNF mutants and serially diluted mouse or human wtTNF (PeproTech EC Ltd., UK) at 4×10^4 cells/well. For neutralization assay, cells were cultured in the presence of a constant concentration of human (20 ng/ml) wtTNF and a serial dilution of TNF mutants. After incubation for 18 h, cell survival was determined by methylene blue assay, as described previously.[21,22] To evaluate the bioactivity of the TNF mutant binding specifically to TNFR2, PC60-hTNFR2 cells were used as an index of granulocyte–macrophage colony-stimulating factor (GM-CSF) production, as described previously.[26] Briefly, PC60-hTNFR2 cells were cultured at 5×10^4 cells/well with interleukin-1β (2 ng/ml) and serially diluted TNF mutant. After 24 h of incubation, the amount of rat GM-CSF produced was quantified by ELISA in accordance with the manufacturer's protocol (R&D Systems, Inc.).

Affinity assessment using SPR

The binding kinetics of wtTNF and TNF mutants were analyzed using the BIAcore 3000 SPR system (GE Healthcare Ltd.). TNFRs were immobilized on a CM5 sensor chip, which resulted in an increase of 3000–5000 resonance units. During the association phase, TNF mutants or wtTNF diluted in HBS-EP running buffer (10 mM HEPES pH7.4, 150 mM NaCl, 3 mM EDTA, 0.005% Tween20, GE Healthcare Ltd.) at 78.4, 26.1, or 8.7 nM were individually passed over the immobilized TNFR at a flow rate of 20 μl/min. During the dissociation phase, HBS-EP buffer was applied to the sensor chip at a flow rate of 20 μl/min. The data were analyzed globally with BIAEVALUATION 3.0 software (GE Healthcare Ltd.) using a 1:1 binding model.

Competitive binding of TNF to TNFR1 and TNFR2 (ELISA)

Goat anti-human IgG (MP Biomedicals, Inc., Solon, OH) was immobilized on Maxisorb 96-well ELISA plates (Nalge Nunc International KK, Japan), and nonspecific binding to the plates was blocked using Block Ace (Dainippon Sumitomo Pharma Co., Ltd., Japan). Human TNFR1-Fc or human TNFR2-Fc (ALEXIS Corporation, Switzerland) was bound to coated antibody. Serially diluted TNF with 50 ng/ml FLAG-tagged wtTNF (wtTNF–FLAG) was added to TNFR1-Fc or TNFR2-Fc in 0.4% Block Ace. wtTNF–FLAG binding was detected by anti-FLAG M2 antibody (Sigma-Aldrich Corporation, St. Louis, MO) and avidin horseradish peroxidase conjugate (Invitrogen Corporation, Carlsbad, CA). The binding affinity of TNF was assessed by competitive wtTNF–FLAG binding to TNFR (IC_{50} value).

X-ray crystallography

Purified R1-6 was concentrated to 10 mg/ml in 20 mM Tris–HCl (pH 7.4). Initial screening using a Hampton Crystal screen 1-2 and Crystal screen Lite kit (Hampton Research Corporation, Aliso Viejo, CA) was performed by vapor diffusion method with hanging drops (1+1 μl) at 20 °C. After optimization of the crystallization conditions, rhombohedral crystals (0.2 mm × 0.2 mm × 0.3 mm) were obtained with reservoir solution containing 0.5 M ammonium sulfate, 1.2 M lithium sulfate, and 0.1 M trisodium citrate (pH 5.6). The crystals were frozen in a cryopreserving solution containing 15% glycerol as cryoprotectant. X-ray diffraction data to 2.5 Å resolution were collected at BL41XU, SPring-8, under flash cooling to 100 K to reduce the effects of radiation damage. Data integration and scaling were performed using HKL2000.[27] Molecular replacement was performed by the MOLREP program in CCP4i[28] using a crystal structure of the wtTNF (1TNF)[25] as search model. Cycles of manual rebuilding using the O program[29] and refinement using the CNS program[30] led to a refined structure. Final refinement (TLS refinement) was performed using the Refmac program in CCP4i.[28] Final model validation was performed using PROCHECK program in CCP4i.[28] The model complexes of TNF–TNFR1 and R1-6–TNFR1 were constructed based on the crystal structure of the LTα–TNFR1 complex[18] using the superimposing program in CCP4i. Structural models of TNFR2 were constructed based on the TNFR1 structure by manual mutation using the O program.[29]

Accession number

Coordinates and structure factors have been deposited in the PDB with accession number 2ZJC.

Acknowledgements

This study was supported by Research for Promoting Technological Seeds (no. 11-067) from the Japan Science and Technology Agency; Research Fund Project on Health Sciences focusing on Drug Innovation (no. KAA3701) from the Japan Health Sciences Foundation; the Global COE Program "*In Silico* Medicine" (Wakate-16) at Osaka University; a Grant-in-Aid for Young Scientists (B) (no. 20790134) and Grants-in-Aid for Scientific Research (nos. 18015055 and 17689008) from the Ministry of Education, Culture, Sports, Science, and Technology of Japan; and Research Fellowships for Young Scientists (no. 20-3919) from the Japan Society for the Promotion of Science.

References

1. Aggarwal, B. B. (2003). Signalling pathways of the TNF superfamily: a double-edged sword. *Nat. Rev. Immunol.* **3**, 745–756.

2. Feldmann, M. & Maini, R. N. (2003). Lasker Clinical Medical Research Award. TNF defined as a therapeutic target for rheumatoid arthritis and other autoimmune diseases. *Nat. Med.* **9**, 1245–1250.
3. Kooloos, W. M., de Jong, D. J., Huizinga, T. W. & Guchelaar, H. J. (2007). Potential role of pharmacogenetics in anti-TNF treatment of rheumatoid arthritis and Crohn's disease. *Drug Discov. Today*, **12**, 125–131.
4. Rutgeerts, P., Van Assche, G. & Vermeire, S. (2004). Optimizing anti-TNF treatment in inflammatory bowel disease. *Gastroenterology*, **126**, 1593–1610.
5. Rothe, J., Lesslauer, W., Lötscher, H., Lang, Y., Koebel, P., Köntgen, F. *et al.* (1993). Mice lacking the tumour necrosis factor receptor 1 are resistant to TNF-mediated toxicity but highly susceptible to infection by *Listeria monocytogenes*. *Nature*, **364**, 798–802.
6. Kafrouni, M. I., Brown, G. R. & Thiele, D. L. (2003). The role of TNF–TNFR2 interactions in generation of CTL responses and clearance of hepatic adenovirus infection. *J. Leukocyte Biol.* **74**, 564–571.
7. Rahman, M. M. & McFadden, G. (2006). Modulation of tumor necrosis factor by microbial pathogens. *PLoS Pathog.* **2**, e4.
8. Chan, F. K., Shisler, J., Bixby, J. G., Felices, M., Zheng, L., Appel, M. *et al.* (2003). A role for tumor necrosis factor receptor-2 and receptor-interacting protein in programmed necrosis and antiviral responses. *J. Biol. Chem.* **278**, 51613–51621.
9. Wajant, H., Pfizenmaier, K. & Scheurich, P. (2003). Tumor necrosis factor signaling. *Cell Death Differ.* **10**, 45–65.
10. Weiss, T., Grell, M., Siemienski, K., Mühlenbeck, F., Dürkop, H., Pfizenmaier, K. *et al.* (1998). TNFR80-dependent enhancement of TNFR60-induced cell death is mediated by TNFR-associated factor 2 and is specific for TNFR60. *J. Immunol.* **161**, 3136–3142.
11. Fotin-Mleczek, M., Henkler, F., Samel, D., Reichwein, M., Hausser, A., Parmryd, I. *et al.* (2002). Apoptotic crosstalk of TNF receptors: TNF-R2-induces depletion of TRAF2 and IAP proteins and accelerates TNF-R1-dependent activation of caspase-8. *J. Cell Sci.* **115**, 2757–2770.
12. Van Ostade, X., Vandenabeele, P., Everaerdt, B., Loetscher, H., Gentz, R., Brockhaus, M. *et al.* (1993). Human TNF mutants with selective activity on the p55 receptor. *Nature*, **361**, 266–269.
13. Barbara, J. A., Smith, W. B., Gamble, J. R., Van Ostade, X., Vandenabeele, P., Tavernier, J. *et al.* (1994). Dissociation of TNF-alpha cytotoxic and pro-inflammatory activities by p55 receptor- and p75 receptor-selective TNF-alpha mutants. *EMBO J.* **13**, 843–850.
14. Van Ostade, X., Vandenabeele, P., Tavernier, J. & Fiers, W. (1994). Human tumor necrosis factor mutants with preferential binding to and activity on either the R55 or R75 receptor. *Eur. J. Biochem.* **220**, 771–779.
15. Van Ostade, X., Tavernier, J. & Fiers, W. (1994). Structure–activity studies of human tumour necrosis factors. *Protein Eng.* **7**, 5–22.
16. Yamagishi, J., Kawashima, H., Matsuo, N., Ohue, M., Yamayoshi, M., Fukui, T. *et al.* (1990). Mutational analysis of structure–activity relationships in human tumor necrosis factor-alpha. *Protein Eng.* **3**, 713–719.
17. Zhang, X. M., Weber, I. & Chen, M. J. (1992). Site-directed mutational analysis of human tumor necrosis factor-alpha receptor binding site and structure–functional relationship. *J. Biol. Chem.* **267**, 24069–24075.
18. Banner, D. W., D'Arcy, A., Janes, W., Gentz, R., Schoenfeld, H. J., Broger, C. *et al.* (1993). Crystal structure of the soluble human 55 kD TNF receptor-human TNF beta complex: implications for TNF receptor activation. *Cell*, **73**, 431–445.
19. Fu, Z. Q., Harrison, R. W., Reed, C., Wu, J., Xue, Y. N., Chen, M. J. & Weber, I. T. (1995). Model complexes of tumor necrosis factor-alpha with receptors R1 and R2. *Protein Eng.* **8**, 1233–1241.
20. Reed, C., Fu, Z. Q., Wu, J., Xue, Y. N., Harrison, R. W., Chen, M. J. & Weber, I. T. (1997). Crystal structure of TNF-alpha mutant R31D with greater affinity for receptor R1 compared with R2. *Protein Eng.* **10**, 1101–1107.
21. Shibata, H., Yoshioka, Y., Ikemizu, S., Kobayashi, K., Yamamoto, Y., Mukai, Y. *et al.* (2004). Functionalization of tumor necrosis factor-alpha using phage display technique and PEGylation improves its anti-tumor therapeutic window. *Clin. Cancer Res.* **10**, 8293–8300.
22. Yamamoto, Y., Tsutsumi, Y., Yoshioka, Y., Nishibata, T., Kobayashi, K., Okamoto, T. *et al.* (2003). Site-specific PEGylation of a lysine-deficient TNF-alpha with full bioactivity. *Nat. Biotechnol.* **21**, 546–552.
23. Shibata, H., Yoshioka, Y., Ohkawa, A., Minowa, K., Mukai, Y., Abe, Y. *et al.* (2008). Creation and X-ray structure analysis of the tumor necrosis factor receptor-1-selective mutant of a tumor necrosis factor-alpha antagonist. *J. Biol. Chem.* **283**, 998–1007.
24. Loetscher, H., Stueber, D., Banner, D., Mackay, F. & Lesslauer, W. (1993). Human tumor necrosis factor alpha (TNF alpha) mutants with exclusive specificity for the 55-kDa or 75-kDa TNF receptors. *J. Biol. Chem.* **268**, 26350–26357.
25. Eck, M. J. & Sprang, S. R. (1989). The structure of tumor necrosis factor-alpha at 2.6 A resolution. Implications for receptor binding. *J. Biol. Chem.* **264**, 17595–17605.
26. Abe, Y., Yoshikawa, T., Kamada, H., Shibata, H., Nomura, T., Minowa, K. *et al.* (2008). Simple and highly sensitive assay system for TNFR2-mediated soluble- and transmembrane-TNF activity. *J. Immunol. Methods*, **335**, 71–78.
27. Otwinowski, Z. & Minor, W. (1997). Processing of X-ray diffraction data collected in oscillation mode. *Methods Enzymol.* **276**, 307–326.
28. Potterton, E., Briggs, P., Turkenburg, M. & Dodson, E. (2003). A graphical user interface to the CCP4 program suite. *Acta Crystallogr. Sect. D*, **59**, 1131–1137.
29. Jones, T. A., Zou, J. Y., Cowan, S. W. & Kjeldgaard, M. (1991). Improved methods for building protein models in electron density maps and the location of errors in these models. *Acta Crystallogr. Sect. A*, **47** (Pt 2), 110–119.
30. Brunger, A. T., Adams, P. D., Clore, G. M., DeLano, W. L., Gros, P., Grosse-Kunstleve, R. W. *et al.* (1998). Crystallography and NMR system: a new software suite for macromolecular structure determination. *Acta Crystallogr. Sect. D*, **54**, 905–921.

Life Sciences 83 (2008) 747–755

Contents lists available at ScienceDirect

Life Sciences

journal homepage: www.elsevier.com/locate/lifescie

Tat conjugation of adenovirus vector broadens tropism and enhances transduction efficiency

Yasuo Yoshioka [a,b,*], Ratima Asavatanabodee [b], Yusuke Eto [b], Hikaru Watanabe [b], Tomohiro Morishige [b], Xinglei Yao [b], Shinya Kida [c], Mitsuko Maeda [c], Yohei Mukai [b], Hiroyuki Mizuguchi [d,e], Koichi Kawasaki [c], Naoki Okada [b], Shinsaku Nakagawa [a,b,*]

[a] The center for Advanced Medical Engineering and Informatics, Osaka University, 1-6, Yamadaoka, Suita, Osaka, 565-0871, Japan
[b] Department of Biotechnology and Therapeutics, Graduate School of Pharmaceutical Sciences, Osaka University, 1-6, Yamadaoka, Suita, Osaka, 565-0871, Japan
[c] Faculty of Pharmaceutical Sciences, Kobe Gakuin University, Nishi-ku, Kobe 651-2180, Japan
[d] Laboratory of Gene Transfer and Regulation, National Institute of Biomedical Innovation, 7-6-8 Saito-Asagi, Ibaraki, Osaka 567-0085, Japan
[e] Graduate School of Pharmaceutical Sciences, Osaka University, 1-6, Yamadaoka, Suita, Osaka, 565-0871, Japan

ARTICLE INFO

Article history:
Received 9 May 2008
Accepted 18 September 2008

Keywords:
Adenovirus
Chemical conjugation
Gene therapy
Macropinocytosis
Protein transduction domain
The coxsackievirus
Adenovirus receptor

ABSTRACT

Aims: Adenovirus vectors (Advs) have been very useful for basic research and clinical gene therapy because they propagate to high titers and efficiently transduce cells and tissues regardless of the mitotic status. However, poor transduction of cells that lack the coxsackievirus and adenovirus receptor (CAR), the primary receptor for Advs, has limited Adv application. In this study, we attempted to generate novel Tat–Advs (Advs conjugated with the HIV Tat-derived peptide, a protein-transduction domain (PTD)) to broaden Adv tropism and enhance transduction efficiency.
Main methods: We constructed Tat–Advs by chemically conjugating Tat peptide to the surface-exposed lysine residues on Advs. We compared the gene transfer activity of Tat–Advs with that of unmodified Advs by measuring the luciferase expression in several types of cell lines.
Key findings: Tat–Advs showed gene expression 1 to 3 log orders higher than unmodified Advs in CAR-negative adherent cells and blood cells, which are refractory to conventional Advs. The inhibition of Tat–Adv-mediated gene expression by heparin and macropinocytosis inhibitor confirms that binding of Tat–Adv to cellular HSPGs and macropinocytosis are essential for efficient CAR-independent transduction. We also demonstrated that Adv modified with another PTD (R8) had the same high transduction efficiency as Tat–Adv.
Significance: These data suggest that Tat–Advs are important tools for transducing cells and will be useful as platform vectors for gene therapy.

Introduction

Gene transduction by viral vectors is currently attracting a great deal of attention for human gene therapy and the functional analysis of genes. In particular, adenovirus vectors (Advs) based on Ad type 5 have been widely used for basic research and clinical gene therapy in vivo and in vitro, because they can be propagated to high titers and efficiently transduce cells and tissues regardless of the mitotic status of the cells (Kaplan, 2005; Kawabata et al., 2006; Roth, 2006). However, the application of Adv in clinical and basic research has been limited by the native tropism of the virus. Entry of Adv into target cells depends on the presence of the coxsackievirus and adenovirus receptor (CAR; the primary receptor for Ad type 5) and integrin coreceptors on the target cells (Wickham et al., 1993; Bergelson et al., 1997; Tomko et al., 1997). Viral binding to the cell surface is mediated by binding of the adenovirus fiber to the CAR on the cells, whereas subsequent internalization occurs by binding of the Arg-Gly-Asp motif in a penton base to αv-integrins. Therefore, Adv cannot efficiently transfer genes of interest into cells lacking CAR expression (e.g., many advanced tumor cells, peripheral blood cells, and hematopoietic stem cells). It is essential to develop novel Advs with efficient transduction independent of the expression of CAR on these cells (Mizuguchi and Hayakawa, 2004; Campos and Barry, 2007).

* Corresponding authors. Yoshioka is to be contacted at The center for Advanced Medical Engineering and Informatics, Osaka University, 1-6, Yamadaoka, Suita, Osaka, 565-0871, Japan. Tel.: +81 6 6879 8177; fax: +81 6 6879 8179. Nakagawa, Department of Biotechnology and Therapeutics, Graduate School of Pharmaceutical Sciences, Osaka University, 1-6, Yamadaoka, Suita, Osaka, 565-0871, Japan. Tel.: +81 6 6879 8175; fax: +81 6 6879 8179.
E-mail addresses: yasuo@phs.osaka-u.ac.jp (Y. Yoshioka), nakagawa@phs.osaka-u.ac.jp (S. Nakagawa).

0024-3205/$ – see front matter © 2008 Elsevier Inc. All rights reserved.
doi:10.1016/j.lfs.2008.09.022

Some proteins, including Tat (transactivator of transcription) of human immunodeficiency virus and the Antennapedia homeodomain proteins of *Drosophila melanogaster* and other species, are taken up by mammalian cells via a receptor-independent unknown pathway (Frankel and Pabo, 1988; Derossi et al., 1994). The domains identified as responsible for this property are referred to as protein transduction domains (PTDs) (Kabouridis, 2003; Murriel and Dowdy, 2006). Most PTDs are 10 to 30 amino acid residues long and enriched in basic amino acids (e.g., arginine and lysine). The Tat peptide with the minimal transduction domain comprising amino acids 48 to 60 of Tat protein (GRKKRRQRRRPPQ) is the most highly investigated PTD. PTDs have been shown to mediate the efficient cellular uptake of a wide variety of cargos, including proteins, peptides, nucleic acids, and even particulates and liposomes with diameters as great as 200 nm (Schwarze et al., 1999; Lewin et al., 2000; Khalil et al., 2006). Recently, several groups reported the utility of PTDs, including the Tat peptide, in Adv-mediated gene transduction (Gratton et al., 2003; Kuhnel et al., 2004; Kurachi et al., 2007). Gratton et al. constructed a complex between Adv and Tat peptide via electrostatic interaction between the high positive charge of Tat peptide and the negative charge of the Adv capsid (Gratton et al., 2003). Their vector, however, requires a high concentration of Tat peptide for efficient gene transfer. Kuhnel et al. bound the Tat peptide to Adv by using fusion proteins consisting of CAR and Tat peptide as an adaptor to Adv (Kuhnel et al., 2004). Kurachi et al. generated genetically modified Advs that contain the Tat peptide in the HI loop of the fiber knob (Kuhnel et al., 2004; Kurachi et al., 2007). These approaches are useful for broadening the tropism of Advs and enhancing transduction efficiency independently of the CAR. However, these approaches are limited to use only with Adv and cannot be applied to other vectors. Therefore, it is important to develop a simple, general method for constructing Tat-modified vectors.

In order to broaden the tropism of Adv and enhance transduction efficiency, we previously developed a system for the synthesis of peptide with a reactive group and generated Tat peptide with 6-maleimidohexanoic acid N-hydroxysuccinimide ester (MHS) (Kida et al., 2006; Kida et al., 2007; Kida et al., 2008). We also succeeded to construct Tat-peptide-conjugated Adv (Tat-Adv) simply, by chemical conjugation of Tat peptide to the surface lysine residues of Adv (Kida et al., 2006; Kida et al., 2008). Here, to optimize Tat-Adv as a vector for gene therapy, we evaluated the relationship between Tat-peptide modification ratio and transduction efficiency. We then examined the gene transfer activities of Tat-Adv in many cell types and the mechanism of cellular uptake of Tat-Adv. We demonstrated that Tat-Adv with optimal modification ratio showed gene expression 1 to 3 log orders higher than unmodified Adv in CAR-negative adherent cells and blood cells, which are refractory to conventional Adv. Furthermore, we confirmed the involvement of the heparan sulfate proteoglycans (HSPGs) and macropinocytosis in the transduction pathway of Tat-Adv. These data suggest that Tat-Adv is an attractive tool for transducing cells and will be useful as a platform vector for gene therapy.

Materials and methods

Cells and animals

A549 cells (human lung carcinoma cells) and U937 cells (histiocytic lymphoma) were purchased from American Type Culture Collection (Manassas, VA); HEK293 (normal human embryonic kidney fibroblasts) were obtained from the Japanese Collection of Research Bioresources (Tokyo, Japan). B16BL6 cells (mouse melanoma cells) were kindly given by Kobegakuin University. CT26 cells (mouse colon carcinoma cells) were provided by Mochida Pharmaceutical Company (Tokyo, Japan). HEK293, A549, RAW264.7 and EL4 cells were cultured in Dulbecco's Modified Eagle Medium (Sigma-Aldrich, St. Louis, MO) containing 10% fetal bovine serum (FBS) and antibiotics. Human glioma cell lines, LN444 (glioblastoma multiforme), LNZ308 (glioblastoma multiforme) and SF295 (glioblastoma multiforme) cells were also cultured in Dulbecco's Modified Eagle Medium containing 10% FBS and antibiotics. B16BL6 and HeLa cells were cultured in Minimal Essential Medium (Sigma-Aldrich) containing 7.5% and 10% FBS, respectively, and antibiotics. CT26 cells were cultured in RPMI-1640 medium (Sigma-Aldrich) containing 10% FBS and antibiotics. U937 cells were cultured in RPMI-1640 medium containing 10 mM HEPES, 1 mM sodium pyruvate, 10% FBS and antibiotics. Female BALB/c mice (age, 5 weeks) were purchased from SLC Inc. (Hamamatsu, Japan). All of the animal experimental procedures were performed in accordance with the Osaka University guidelines for the welfare of animals.

Development of adenovirus vectors

E1-deleted adenovirus type 5 expressing firefly luciferase or EGFP under the control of cytomegalovirus promoter was constructed by an improved in vitro ligation method as previously reported (Mizuguchi and Kay, 1998; Mizuguchi and Kay, 1999). Each Adv was amplified in 293 cells using established methods, purified from cell lysates by banding twice through CsCl gradients, dialyzed, and stored at −80 °C (Lu et al., 1998). The virus particle titer was determined spectrophotometrically by the methods of Maizel et al. (1968). The ratio of the particle-to-biological titer was between 10 and 40.

Construction of reactive Tat peptide

The scheme used to synthesize reactive Tat peptide is shown in Fig. 1a. We used a derivative of Tat peptide containing the cross-linking reagent MHS, which reacts with amine and sulfhydryl moieties. The peptide was synthesized with an Applied Biosystems Peptide Synthesizer 433A-1 (Applied Biosystems, Foster City, CA, USA). 9-Fluorenylmethoxycarbonyl (Fmoc) amino acids [Fmoc-Gly-OH; Fmoc-Pro-OH; N^{α}-Fmoc-N^{G}-2,2,4,6,7-pentamethyldihydrobenzofuran-5-sulfonylarginine: Fmoc-Arg(Pbf)-OH; N^{α}-Fmoc-S-tritylcysteine: Fmoc-Cys(Trt)-OH; N^{α}-Fmoc-N^{ϵ}-t-butoxycarbonyl-lysine: Fmoc-Lys(Boc)-OH; and N^{α}-Fmoc-N^{γ}-tritylglutamine: Fmoc-Gln(Trt)-OH] were coupled in a stepwise manner to Rink amide resin (PE Biosystems, Amino content: 0.67 mequiv/g, 379 mg, 0.25 mmol) using the coupling reagent, 2-(1-H-benzotriazole-1-yl)1,1,3,3-tetramethyluronium hexafluorophosphate (HBTU), in N-methylpyrrolidone (NMP). After each coupling step, the Fmoc group was removed by using 20% piperidine/NMP. The synthetic Fmoc-Gly-Arg(Pbf)-Lys(Boc)-Lys(Boc)-Arg(Pbf)-Arg(Pbf)-Gln(Trt)-Arg (Pbf)-Arg(Pbf)-Arg(Pbf)-Pro-Pro-Gln(Trt)-Gly-Cys(Trt)-Rink amide resin was treated with 20% piperidine/NMP and then treated with acetic anhydride. The peptide was cleaved from the resin with trifluoroacetic acid (TFA)/H_2O/triisopropylsilane (95:2.5:2.5). Since synthesized peptide was deprotected and removed from resin with TFA, the ε-amino group of Lys forms the TFA salt and provided the next reaction step. The resulting crude peptide, (Ac-GRKKRRQRRRPPQGC-NH_2), was purified by RP-HPLC. The purified peptide, dissolved in PBS, and MHS, dissolved in dimethylsulfoxide, were combined and then stirred for 30 min. The product, Ac-GRKKRRQRRRPPQGC-MHS (Tat-MHS), was frozen immediately at −80 °C.

Covalent attachment of Tat to Adv

Conventional Advs were reacted with a 12.5-, 25-, 50-, or 100-fold molar excess of Tat-MHS to viral lysine residue at 37 °C for 40 min, with gentle stirring. The conjugation of Tat-MHS to Adv was determined by SDS-PAGE analysis. SDS-PAGE was carried out under reducing conditions in a gradient gel containing 4% to 20% polyacrylamide (PAG Mini 4/20, Daiichi Pure Chemicals, Tokyo, Japan) and gel was stained for the viral protein hexon by use of Coomassie blue.

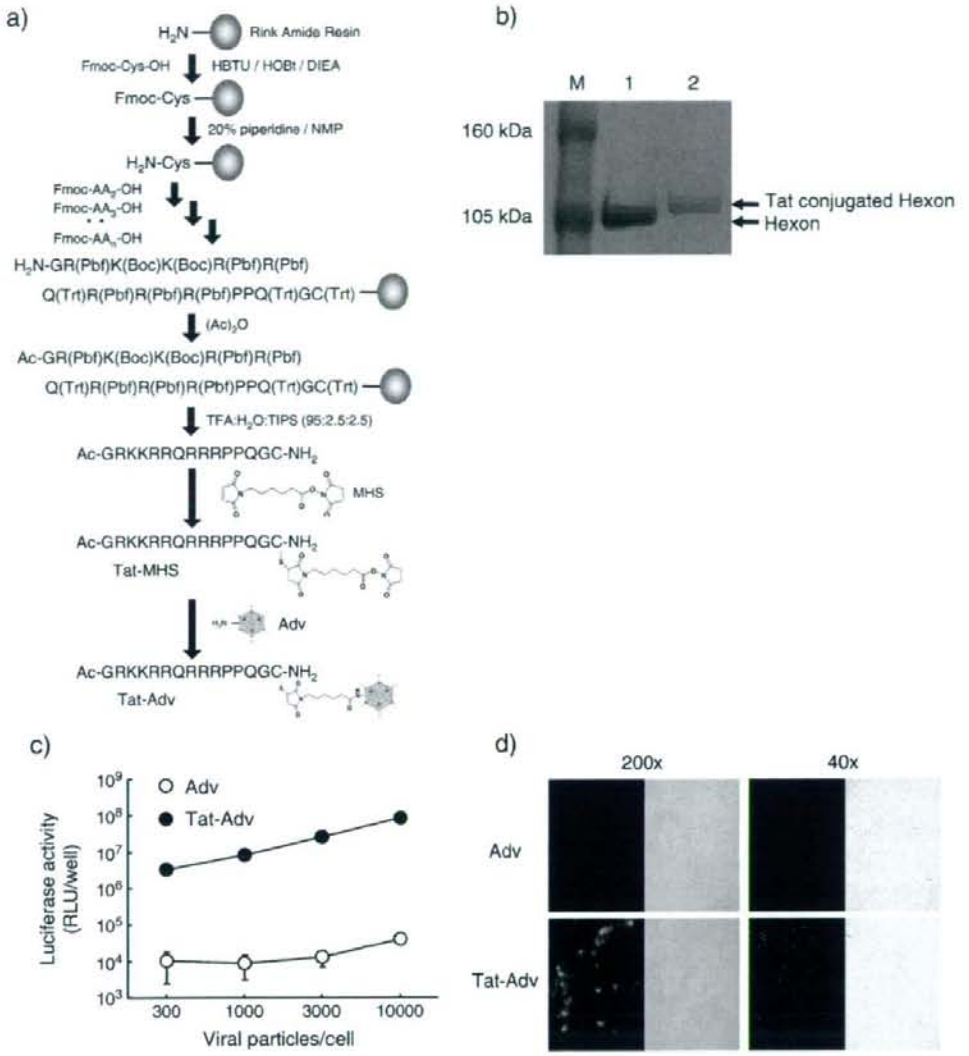

Fig. 1. Efficiency of transduction of Tat–Adv into B16BL6 cells. (a) Tat–Adv was constructed by the scheme. (b) SDS-PAGE analysis of Tat–Adv. SDS-PAGE analysis of Tat–Adv was conducted under reducing conditions and the gel was stained with Coomassie blue. Lane M, protein marker; lane 1, Adv; lanes 2, Tat–Adv. (c) B16BL6 cells (1×10^4 cells) were transduced with 300, 1000, 3000, or 10,000 vp/cell of Adv or Tat–Adv encoding the luciferase gene. After 24 h of cultivation, luciferase expression was measured. Each point represents the mean ± SD. (d) B16BL6 cells (1×10^4 cells) were transduced with 10,000 vp/cell of Adv or Tat–Adv encoding the EGFP gene. After 24 h of cultivation, EGFP expression was determined by fluorescence microscopy. Magnification, 200×, 40×.

Adenovirus-mediated gene transduction into adherent cells

Adherent cells (1×10^4 cells/well) were seeded onto a 48-well plate. On the following day, they were transduced with 300, 1000, 3000, or 10,000 vector particles (vp)/cell of Adv or Tat–Adv in a final volume of 400 μl in culture medium. After 24 h of cultivation, luciferase activity was measured with a Luciferase Assay System (Promega, Madison, WI, USA) and a Lumat LB 9507 luminometer (EG&G Berthold, Bad Wildbad, Germany) in accordance with the manufacturers' instructions after the cells had been lysed with Luciferase Cell Culture Lysis Reagent (Promega). Luciferase activity was calculated as relative light units (RLU)/well. To evaluate the expression of EGFP, B16BL6 cells (1×10^4 cells/well) were transduced with 10,000 vp/cell of Adv or Tat–Adv encoding EGFP gene. After 24 h of cultivation, expression of EGFP was measured by BZ-8000 (KEYENCE, Tokyo, Japan) Luciferase Assay System (Promega, Madison, WI, USA).

Adenovirus-mediated gene transduction into blood cells

Blood cells (2×10^4 cells/well) were seeded onto a 48-well plate. They were then transduced with 10,000 vp/cell of Adv or Tat–Adv in a final volume of 200 μl in culture medium. After 24 h cultivation, luciferase

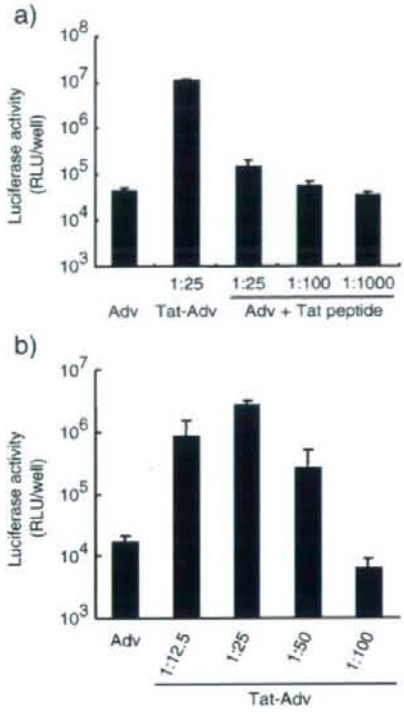

Fig. 2. Optimum condition or density of Tat peptide on the surface of Adv. (a) Comparison of efficiencies of transduction by Tat–Adv and by Adv mixed with Tat peptide containing no MHS. B16BL6 cells (1×10^4 cells) were transduced with each Adv at 10,000 vp/cell. After 24 h of cultivation, luciferase expression was measured. Each bar represents the mean ± SD. Tat–Adv, molar ratio of 1:25 (Adv:Tat–MHS); Adv mixed with Tat peptide containing no MHS, molar ratios of 1:25, 1:100, 1:1000 (Adv: Tat-peptide containing no MHS). (b) Efficiency of transduction of Tat–Adv with various modification ratios. B16BL6 cells (1×10^4 cells) were transduced with Adv or Tat–Adv at 1000 vp/cell with various modification ratios. After 24 h of cultivation, luciferase expression was measured. Each bar represents the mean ± SD. Tat–Adv, molar ratios of 1:12.5, 1:25, 1:50, 1:100 (Adv:Tat–MHS).

activity was measured with a Bright-Glo Luciferase Assay System (Promega) and a Lumat LB 9507 luminometer in accordance with the manufacturers' instructions. Luciferase activity was calculated as RLU/well.

Comparison of transduction efficiencies of Tat–Adv and Adv mixed with Tat peptide

B16BL6 cells (1×10^4 cells/well) were seeded onto a 48-well plate. The following day, Adv was incubated with free Tat peptides (1:25, 1:100, or 1:1000) for 40 min at 37 °C. Then, B16BL6 cells were transduced with 10,000 vp/cell of Adv, Tat–Adv, or Adv mixed with Tat-peptide containing no MHS in a final volume of 400 μl in culture medium. After 24 h cultivation, luciferase activity was measured by the Luciferase Assay System and a Lumat LB 9507 luminometer after the cells were lysed with Luciferase Cell Culture Lysis Reagent. Luciferase activity was calculated as RLU/well.

Preparation of adenovirus vector antiserum

Adv antiserum was obtained from BALB/c mice. In brief, a dose of 5×10^{10} vp of unmodified Adv was administered intravenously to a female BALB/c mouse (age, 5 weeks). Two weeks later, an additional dose of 5×10^{10} vp was intravenously administered. Mouse serum was collected after 2 weeks and stored at −80 °C.

Neutralizing antibody evasion ability of Tat–Adv

A549 cells (1×10^4 cells/well) were seeded onto a 48-well plate. The following day, the cells were transduced with 10,000 vp/cell of Adv or Tat–Adv in the presence or absence of 3200- or 12,800-fold diluted Adv antiserum (final volume, 200 μl). After 24 h of cultivation, luciferase activity was measured.

CAR dependency of cellular uptake of Tat–Adv

A549 cells (1×10^4 cells/well) were seeded onto a 48-well plate. The following day, A549 cells were pretreated with or without 1 μg/ml of mouse anti-CAR IgG (Upstate, Charlottesville, VA, USA) for 1 h. The A549 cells were then transduced with Adv or Tat–Adv at 10,000 vp/cell (final volume, 200 μl). After 24 h of cultivation, luciferase activity was measured.

HSPGs-dependency of cellular uptake of Tat–Adv

A549 cells (1×10^4 cells/well) were seeded onto a 48-well plate. The following day, the cells were transduced with Adv or Tat–Adv at 10,000 vp/cell in culture medium in the presence or absence of 6.25, 25, or 100 μg/ml of heparin sodium salt (Sigma-Aldrich) (final volume, 200 μl). After 2 h, the virus solution was replaced with fresh medium. After 24 h of cultivation, luciferase activity was measured.

Macropinocytosis-dependency of cellular uptake of Tat–Adv

A549 cells (1×10^4 cells/well) were seeded onto a 48-well plate. The following day, A549 cells were pretreated for 30 min with or without 2.5 mM amiloride HCl hydrate (Sigma-Aldrich) as a macropinocytosis inhibitor. The A549 cells were then transduced with Adv or Tat–Adv at 1000 vp/cell (final volume, 200 μl). After 30 min, the virus solution was replaced with fresh medium. After 24 h of cultivation, luciferase activity was measured.

Statistical analysis

All results are expressed as mean ± SEM or SD. Differences were compared using Student *t*-tests or Scheffe's method after analysis of variance (ANOVA).

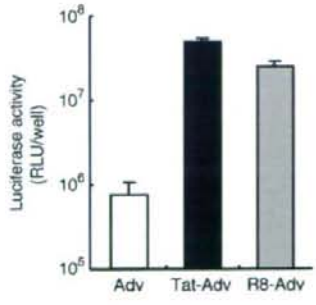

Fig. 3. Efficiency of transduction of R8–Adv. B16BL6 cells (1×10^4 cells) were transduced with 10,000 vp/cell of Adv, Tat–Adv, or R8–Adv encoding the luciferase gene. After 24 h of cultivation, luciferase expression was measured. Each bar represents the mean ± SD.

Results

Generation and properties of Tat–Adv

For chemical conjugation of Tat peptide to Adv, we synthesized Tat–MHS (Fig. 1a). The Tat peptide was synthesized by the solid phase method and then coupled to the MHS. We used a derivative of Tat peptide in which cysteine residue was added to the C-terminus of the peptide. Cysteine was added so that the peptide could be linked to Adv through the heterofunctional cross-linking reagent MHS, which reacts with amine and sulfhydryl moieties. To construct Tat–Adv by using Tat–MHS, Adv was reacted with Tat–MHS at a molar ratio of 1:25 (Adv:

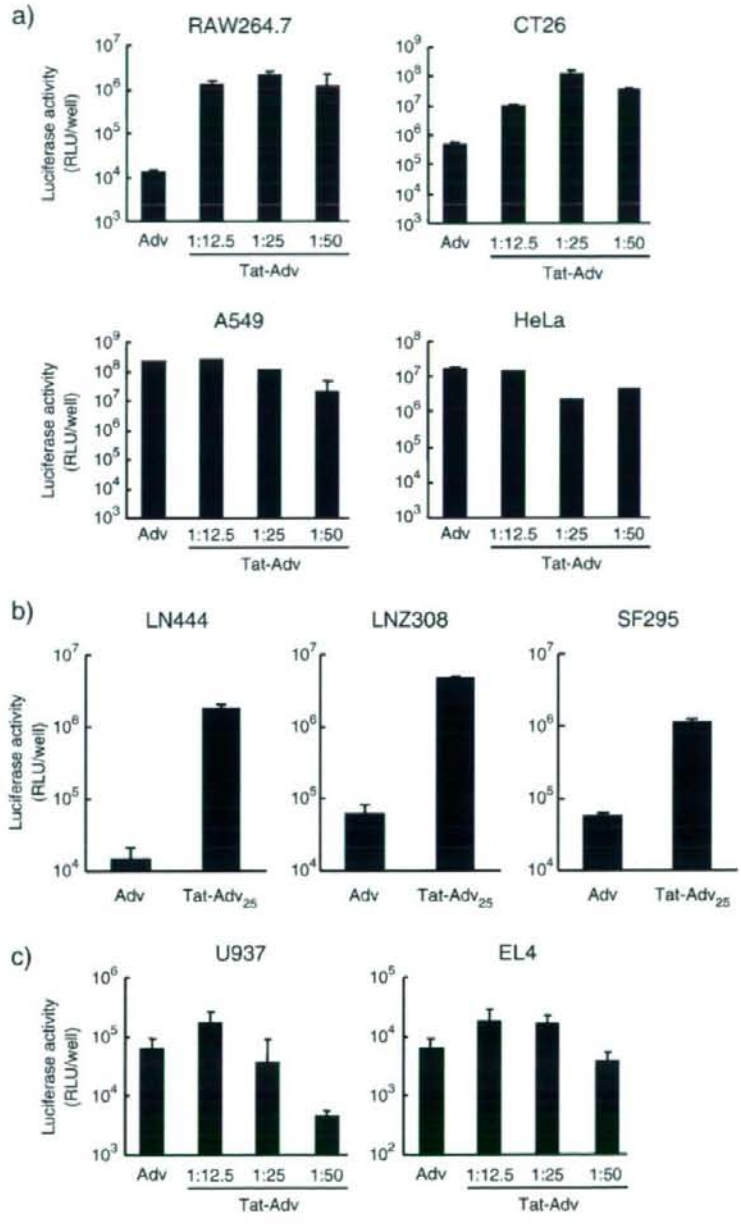

Fig. 4. Gene transfer activities of Tat–Adv in several types of cell lines. (a) RAW264.7, CT26, A549, HeLa (1×10^4 cells), (b) LN444, LNZ308, SF295 (1×10^4 cells) and (c) U937 and EL4 cells (2×10^4 cells) were transduced with 10,000 vp/cell of Adv or Tat–Adv encoding the luciferase gene. After 24 h of cultivation, luciferase expression was measured. Each bar represents the mean ± SD. Tat–Adv, molar ratio of 1:12.5, 1:25, 1:50 (Adv:Tat–MHS).

Tat–MHS) (Fig. 1a). Because conjugation of Tat–MHS to Adv results in modification of lysine residues on the capside proteins, such as the Adv hexon, fiber, and penton base, we confirmed that Tat–MHS conjugated hexon, the main capsid protein of Adv, by SDS-PAGE with Coomassie brilliant blue staining (Fig. 1b).

To investigate the transduction efficiency of Tat–Adv, we compared the gene transfer activity of Tat–Adv with that of unmodified Adv by using luciferase-expressing Advs in B16BL6 cells. B16BL6 cells are CAR-negative, and it is difficult to obtain sufficient gene expression by Adv (Koizumi et al., 2001; Koizumi et al., 2003). Tat–Adv showed 2 to 3 log orders higher luciferase expression than unmodified Adv in a vector particle-dependent manner (Fig. 1c). In addition, the efficiency of transduction in B16BL6 cells was evaluated by fluorescence microscopy using enhanced green fluorescence protein (EGFP)-expressing Advs. Visualization of cells by fluorescence microscopy showed that more Tat–Adv-treated cells than unmodified Adv-treated cells were EGFP positive (Fig. 1d). Approximately half the cells treated with Tat–Adv in the field of view showed bright-green fluorescence, whereas cells treated with unmodified Adv showed only background fluorescence. In a separate experiment, we showed that cell viability was not affected by transduction with either Adv type under these experimental conditions (data not shown).

Tat peptide is rich in basic residues and has a high positive charge. Therefore, Tat peptide should interact with the negative charge of the Adv capsid via an electrostatic interaction. To investigate the significance of direct covalent binding of Tat peptide to Adv for gene transfer, we compared the luciferase expression of Tat–Adv with that of Adv merely mixed with Tat peptide. Adv mixed with Tat peptide containing no MHS showed no increase in luciferase expression compared with unmodified Adv, whereas the luciferase expression of Tat–Adv generated by Tat–MHS at the same Tat to Adv ratio as used in the mixture was 250 times higher than that of unmodified Adv (Fig. 2a). These data indicated that direct chemical binding of Tat–MHS to Adv was essential for a high rate of transduction of Tat–Adv.

To assess the effect of Tat-peptide density on transduction efficiency, we constructed several types of Tat–Adv in which the modification ratio of the Tat peptide differed. Adv was reacted with increasing amounts of Tat–MHS; we then compared the luciferase expression in B16BL6 cells. Tat–Adv with a reaction ratio between 1:12.5 and 1:50 (Adv:Tat–MHS) showed markedly higher luciferase expression than unmodified Adv, but Tat–Adv with a reaction ratio of 1:100 (Adv:Tat–MHS) showed lower luciferase expression than unmodified Adv (Fig. 2b). These data indicated that there are optimal reaction conditions for improved transduction by Tat–Adv.

Homopolymers of arginine, called octaarginine (R8) peptide, are similar to Tat peptide in terms of efficiency and uptake mechanism, making them possible candidates for mimicking the Tat peptide (Futaki, 2005; Futaki et al., 2007). We assessed whether R8 peptide had effects similar to those of Tat peptide on Adv infection (Fig. 3). In B16BL6 cells, R8-peptide-conjugated Adv (R8–Adv) showed 30 times higher luciferase expression than unmodified Adv, indicating that higher transductional ability may be a common feature of PTDs.

Transduction efficiencies of Tat–Adv in several types of cells

Next, we examined the gene transfer activities of Tat–Adv in several types of adherent cell lines (Fig. 4a and b). We also compared the transduction efficiencies of Tat–Adv with the reaction ratios 1:12.5, 1:25, and 1:50 (Adv:Tat–MHS) (Tat–$Adv_{12.5}$, Tat–Adv_{25} and Tat–Adv_{50} respectively). Raw264.7, CT26, LN444, LNZ308 and SF295 cells were CAR-negative, whereas A549 and HeLa cells were CAR-positive (Koizumi et al., 2001; Okada et al., 2001b; Emile Gras et al., 2006). The luciferase expression in the CAR-negative adherent cell lines (Raw264.7 and CT26) transduced with Tat–Advs at any of the ratios was approximately 2 log orders higher than that observed with unmodified Adv (Fig. 4a). In the CAR-positive adherent cell lines (A549 and Hela), all Tat–Advs showed luciferase expression as efficient as that of unmodified Adv (Fig. 4a). In addition, Tat–Adv_{25} showed 1–2 log orders higher luciferase expression than unmodified Adv in CAR-negative adherent human glioma cells (LN444, LNZ308 and SF295) (Fig. 4b). Next we investigated the gene transfer activities of Tat–Advs in blood cells (U937 and EL4) (Fig. 4c). Blood cells are well known to be refractory to Adv-mediated transduction (Koizumi et al., 2001). In U937 and EL4 cells, Tat–$Adv_{12.5}$ mediated luciferase expression at a rate 3 times higher than did unmodified Adv, whereas luciferase expression by Tat–Adv_{25} and Tat–Adv_{50} was similar to, or lower than, that observed with unmodified Adv. These results indicated that Tat–Adv improved transduction efficiency in many cell types, including blood cells.

Internalization mechanisms of Tat–Adv

One potential limiting factor associated with Adv gene therapy is the existence of anti-Adv neutralizing antibodies (Abs), which limit the repeat administration of Adv (Hemminki et al., 2002; Barouch et al., 2004; Sumida et al., 2005). Most adults have low levels of anti-Adv neutralizing Abs, which hamper efficient Adv-mediated gene transfer. To investigate whether Tat–Adv was protected against anti-Adv neutralizing Abs, in vitro neutralization assay was performed to determine whether Tat–Adv had transduction efficiency in the presence of neutralizing Abs. Tat–Adv was significantly less susceptible to neutralization than unmodified Adv at both concentrations of anti-Adv serum tested (Fig. 5). This suggests that the availability of the virion surface epitopes to Abs is markedly reduced, presumably because of the shielding of antibody binding sites by Tat peptides.

To investigate the mechanism of cellular uptake of Tat–Adv, we compared the gene expression of Tat–Adv in the presence or absence of anti-CAR Ab. In CAR-positive A549 cells, luciferase expression in the cells transduced with unmodified Adv in the presence of anti-CAR Ab was 50% less than that in the absence of anti-CAR Ab. In contrast, the cells transduced with Tat–Adv in the presence of anti-CAR Ab showed a high level of gene expression similar to that in the absence of anti-CAR Ab, indicating that the cellular uptake of Tat–Adv is independent of CAR, and that Tat–Adv is taken up by the cell via an alternative mechanism (Fig. 6a). It has been shown that positively charged PTDs adhere to HSPGs on cell surfaces and that this interaction can be inhibited by negatively charged heparin (Console et al., 2003; Richard et al., 2005). Subsequent events are needed for internalization, and it has been proposed that macropinocytosis is a major pathway for the

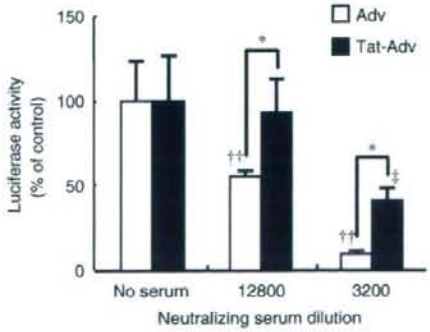

Fig. 5. Antibody evasion ability of Tat–Adv. A549 cells (1×10^4 cells) were transduced with Adv or Tat–Adv at 10,000 vp/cell in the presence or absence of Adv antiserum. After 24 h of cultivation, luciferase expression was measured. Each bar represents the mean ± SD. (*; $P<0.05$ by Student's *t*-test. ††; $P<0.01$ versus value for Adv in the absence of Adv antiserum by ANOVA. ‡; $P<0.05$ versus value for Tat–Adv in the absence of Adv antiserum by ANOVA.)

endocytic uptake of PTDs (Nakase et al., 2004; Wadia et al., 2004; Kaplan et al., 2005). To investigate the involvement of Tat binding to HSPGs in Tat–Adv-mediated transduction, we treated cells with increasing doses of heparin. Heparin significantly inhibited Tat–Adv-mediated luciferase expression in a dose-dependent manner, whereas unmodified Adv-mediated gene expression was not changed (Fig. 6b). Next, to investigate whether Tat–Adv could infect cells through macropinocytosis, we examined the effects of the macropinocytosis inhibitor amiloride on transduction efficiency. Pretreatment with amiloride decreased the luciferase expression of Tat–Adv but had no effect on the luciferase expression of unmodified Adv (Fig. 6c). The inhibition of Tat–Adv-mediated gene expression by heparin and by macropinocytosis inhibitor confirms that both binding of Tat–Adv to cellular HSPGs and macropinocytosis are essential for Tat–Adv-mediated efficient transduction.

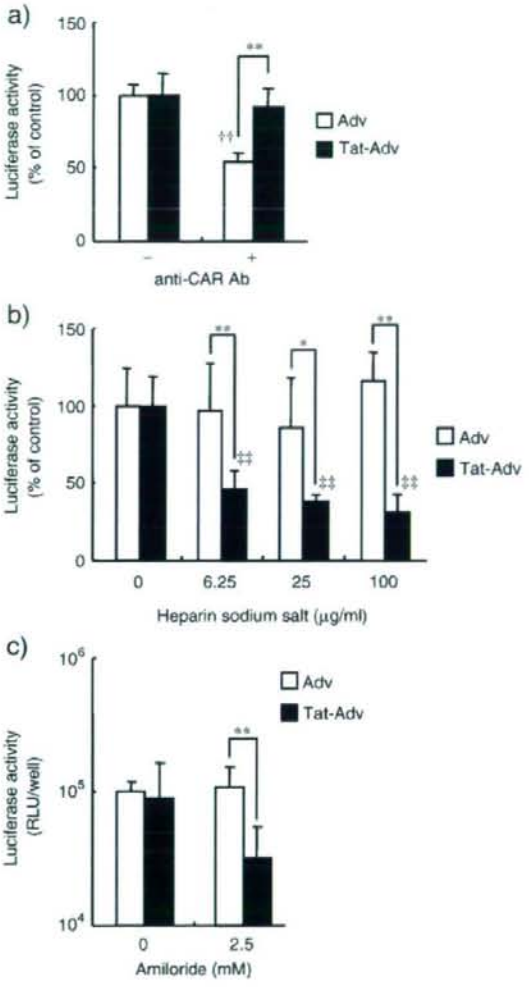

Fig. 6. Cell-entering mechanism of Tat–Adv. (a) Comparison of CAR dependency of cellular uptake of Adv and Tat–Adv. A549 cells (1×10^4 cells) were preincubated for 1 h with anti-CAR Ab at 1 μg/ml. Then, A549 cells were transduced with Adv or Tat–Adv at 10,000 particles/cell. After 24 h of cultivation, luciferase expression was measured. Each bar represents the mean ± SD. (**; $P<0.01$ by Student's *t*-test, ††; $P<0.01$ versus value for Adv in the absence of anti-CAR Ab by Student's *t*-test). (b) HSPGs dependency of cellular uptake of Tat–Adv. A549 cells (1×10^4 cells) were incubated with Adv or Tat–Adv at 10,000 vp/cell in the presence or absence of heparin sodium salt at 6.25, 25, or 100 μg/ml. After 2 h, the virus solution was replaced with fresh medium. After 24 h of cultivation, luciferase expression was measured. Each bar represents the mean ± SD. (*; $P<0.05$, **; $P<0.01$ by Student's *t*-test, ‡‡; $P<0.01$ versus value for Tat–Adv in the absence of heparin sodium salt by ANOVA.). (c) Macropinocytosis dependency of cellular uptake of Tat–Adv. A549 cells (1×10^4 cells) were pretreated for 30 min with or without amiloride at 2.5 mM. Then, A549 cells were transduced with Adv or Tat–Adv at 1000 vp/cell. After 30 min, the virus solution was replaced with fresh medium. After 24 h of cultivation, luciferase expression was measured. Each bar represents the mean ± SD (* $P<0.05$).

Discussion

One of the hurdles confronting Adv-mediated gene transfer is that infection with Adv is dependent on the expression levels of the CAR. As a consequence, expression of the CAR determines viral tropism and frequently limits effective gene delivery by Adv. For example, because many tumor cells, including melanoma, that are targets for gene therapy express no or little CAR, it is difficult to achieve sufficient gene expression and therapeutic effect (Okada et al., 2003b; Mathis et al., 2006). Reduced expression of CAR in advanced tumor stages is one of the major obstacles to the use of Adv for cancer gene therapy (Yamamoto et al., 1997; Li et al., 1999; Yamashita et al., 2007). To overcome these problems, we developed Tat-modified Adv with broadened tropism and enhanced transduction efficiency.

Previously, we developed a system for the synthesis of peptide with a reactive group and succeeded in generating Tat–MHS (Kida et al., 2006, 2007, 2008). We prepared Tat–Adv by a simple procedure, mixing Adv with Tat–MHS (Fig. 1a). Tat–Adv showed 2 to 3 log orders higher gene expression than unmodified Adv in CAR-negative adherent cells (B16BL6, Raw264.7, CT26, LN444, LNZ308 and SF295), whereas the luciferase expression of Tat–Adv was similar to that of unmodified Adv in CAR-positive adherent cells (A549 and Hela) (Figs. 1c, 4a and b). In addition, Tat–Adv showed transgene expression several times higher than that of unmodified Adv in blood cells (U937 and EL4) (Fig. 4c). We also examined the relationship between the modification ratio of Tat peptide and transduction efficiency. Tat–Adv at reaction ratios between 1:12.5 and 1:50 (Adv:Tat–MHS) showed the highest luciferase expression, and further increases in the modification ratio of Tat peptide generated expression lower than that with unmodified Adv in B16BL6 cells (Fig. 2b). These results suggested that there is an optimum modification ratio of Tat peptide for the efficient transduction of Tat–Adv.

We focused on how the style of modification of Tat peptide affects Adv-mediated gene expression activity. We showed that modification by Tat-peptide without MHS failed to improve the transduction efficiency of Adv in B16BL6 cells (Fig. 2a). Gratton et al. obtained results opposite from ours (Gratton et al., 2003). They succeeded in improving transduction just by mixing Adv with Tat peptide containing no MHS. However, they constructed a complex between Adv and Tat peptide with a reaction ratio of 1:100,000 (Adv:peptides) — 4000 times higher than our ratio. We used Tat–Adv with a reaction ratio of 1:25 (Adv:Tat–MHS) to obtain significant effects. These results indicated that specific binding of Tat peptide to the viral particle requires less Tat peptide than when Adv is simply mixed with Tat peptide containing no MHS; this specific binding is necessary for efficient PTD-mediated transduction of Tat–Adv.

Recent data have demonstrated that internalization of Tat fusion protein and Tat-modified liposome as well as that of Tat peptide occur mainly through macropinocytosis (Nakase et al., 2004; Wadia et al., 2004; Kaplan et al., 2005; Richard et al., 2005; Khalil et al., 2006; Tunnemann et al., 2006). It has been suggested that macropinocytosis is a major pathway for the endocytic uptake of PTDs. We showed that Tat–Adv was also mainly internalized by macropinocytosis in A549 cells (Fig. 6c). Macropinocytosis involves the formation of large heterogeneous macropinosomes. Although the exact nature of Tat-mediated

release from macropinosomes into the cytosol remains unclear, macropinosomes are thought to be vesicles that are inherently leakier than other types of endosomes (Meier et al., 2002). Therefore, we speculated that the internalized Tat–Adv is easily released to the cytosol and move toward the nucleus, resulting in efficient gene expression.

Cell-surface proteoglycans such as HSPGs have been suggested to be primary receptors for the cellular uptake of PTDs, and a deficiency of HSPG often results in a decrease in the amount of PTDs taken up by the cells, although some reports have shown that HSPG is not involved in the cellular uptake of PTDs (Console et al., 2003; Richard et al., 2005; Rothbard et al., 2005; Nakase et al., 2007). Cell-surface HSPGs are also reported to be indispensable for the induction of actin organization and the macropinocytic uptake of PTDs (Nakase et al., 2004, 2007). Our results demonstrated that the presence of heparin in the medium dramatically inhibited the transduction of Tat–Adv in A549 cells (Fig. 6b), suggesting that the presence of cell-surface HSPG may be important for cellular binding and macropinocytic uptake of Tat–Adv. Recently it was shown that Tat-linked Adv, in which Tat peptide was bound to Adv by using fusion proteins consisting of CAR and the Tat peptide as an adaptor to Adv, enters the cells via HSPG (Kuhnel et al., 2004). Han et al. also showed that genetic incorporation of the Tat peptide into Adv fiber allowed to infect cells via HSPG (Han et al., 2007). These results are consistent with our observation. However, Kurachi et al. reported that the transduction of Adv genetically modified with Tat peptide, in which Tat peptide was introduced into the HI loop of the fiber knob, is not inhibited by heparinase, indicating that the genetically modified Adv transduces into the cells independently of HSPG (Kurachi et al., 2007). The precise reason for these contradictory results remains unclear. Now we are trying to examine the more precise cellular uptake mechanism of Tat–Adv using other macropinocytosis inhibitor and proteoglycan-deficient cells.

We also demonstrated that R8–Adv showed luciferase expression as high as that of Tat–Adv in B16BL6 cells (Fig. 3), indicating the usefulness of other PTDs in our PTD-conjugated Adv system. Recently, many artificial PTDs with high cell-penetrating ability have been developed (Ho et al., 2001; Mukai et al., 2006). We should be able to generate PTD-modified Advs by using these novel PTDs.

Tat–Adv has advantages over conventional Adv in many clinical applications. For example, we have shown that dendritic cell (DC)-based ex vivo immunotherapy genetically modified by Adv is useful, but the transduction efficiency of conventional Adv is insufficient for clinical use because of the lack of CAR expression on the DC surface (Okada et al., 2001a, 2003a). We consider that Tat–Adv is likely to be powerful tool for DC-based immunotherapy. In addition, for in vivo cancer gene therapy, intra-tumoral injection of Tat–Adv could enhance Adv transduction in tumor tissues and reduce side effects because of the lower dose of Adv injected, although gene transduction in vivo is affected by several cellular and humoral factors (Kurachi et al., 2007). We are now investigating the usefulness of Tat–Adv for these applications.

Conclusion

In summary, to broaden the tropism of Adv and enhance transduction efficiency, we generated Tat-modified Adv by simple chemical conjugation methods. The Tat–Adv improved transgene expression in CAR-negative cells in an HSPG- and macropinocytosis-dependent manner. This method could also be applied to other virus vectors. Tat-peptide-modified Adv is an attractive tool for transducing cells and can be useful as a platform vector for gene therapy and basic research.

Acknowledgements

The authors declare no conflict of interests. This study was supported in part by grants from the Ministry of Health, Labor, and Welfare in Japan, by the Research on Health Sciences focusing on Drug Innovation from the Japan Health Sciences Foundation and by the Mochida Memorial Foundation for Medical and Pharmaceutical Research.

References

Barouch, D.H., Pau, M.G., Custers, J.H., Koudstaal, W., Kostense, S., Havenga, M.J., Truitt, D.M., Sumida, S.M., Kishko, M.G., Arthur, J.C., Korioth-Schmitz, B., Newberg, M.H., Gorgone, D.A., Lifton, M.A., Panicali, D.L., Nabel, G.J., Letvin, N.L., Goudsmit, J., 2004. Immunogenicity of recombinant adenovirus serotype 35 vaccine in the presence of pre-existing anti-Ad5 immunity. Journal of Immunology 172, 6290–6297.

Bergelson, J.M., Cunningham, J.A., Droguett, G., Kurt-Jones, E.A., Krithivas, A., Hong, J.S., Horwitz, M.S., Crowell, R.L., Finberg, R.W., 1997. Isolation of a common receptor for Coxsackie B viruses and adenoviruses 2 and 5. Science 275, 1320–1323.

Campos, S.K., Barry, M.A., 2007. Current advances and future challenges in Adenoviral vector biology and targeting. Current Gene Therapy 7, 189–204.

Console, S., Marty, C., Garcia-Echeverria, C., Schwendener, R., Ballmer-Hofer, K., 2003. Antennapedia and HIV transactivator of transcription (TAT) "protein transduction domains" promote endocytosis of high molecular weight cargo upon binding to cell surface glycosaminoglycans. Journal of Biological Chemistry 278, 35109–35114.

Derossi, D., Joliot, A.H., Chassaing, G., Prochiantz, A., 1994. The third helix of the Antennapedia homeodomain translocates through biological membranes. Journal of Biological Chemistry 269, 10444–10450.

Emile Gras, J.C., Verkuijlen, P., Frants, R.R., Havekes, L.M., van Berkel, T.J., Biessen, E.A., van Dijk, K.W., 2006. Specific and efficient targeting of adenovirus vectors to macrophages: application of a fusion protein between an adenovirus-binding fragment and avidin, linked to a biotinylated oligonucleotide. Journal of Gene Medicine 8, 668–678.

Frankel, A.D., Pabo, C.O., 1988. Cellular uptake of the tat protein from human immunodeficiency virus. Cell 55, 1189–1193.

Futaki, S., 2005. Membrane-permeable arginine-rich peptides and the translocation mechanisms. Advanced Drug Delivery Reviews 57, 547–558.

Futaki, S., Nakase, I., Tadokoro, A., Takeuchi, T., Jones, A.T., 2007. Arginine-rich peptides and their internalization mechanisms. Biochemical Society Transactions 35, 784–787.

Gratton, J.P., Yu, J., Griffith, J.W., Babbitt, R.W., Scotland, R.S., Hickey, R., Giordano, F.J., Sessa, W.C., 2003. Cell-permeable peptides improve cellular uptake and therapeutic gene delivery of replication-deficient viruses in cells and in vivo. Natural Medicines 9, 357–362.

Han, T., Tang, Y., Ugai, H., Perry, L.E., Siegal, G.P., Contreras, J.L., Wu, H., 2007. Genetic incorporation of the protein transduction domain of Tat into Ad5 fiber enhances gene transfer efficacy. Journal of Virology 4, 103.

Hemminki, A., Wang, M., Desmond, R.A., Strong, T.V., Alvarez, R.D., Curiel, D.T., 2002. Serum and ascites neutralizing antibodies in ovarian cancer patients treated with intraperitoneal adenoviral gene therapy. Human Gene Therapy 13, 1505–1514.

Ho, A., Schwarze, S.R., Mermelstein, S.J., Waksman, G., Dowdy, S.F., 2001. Synthetic protein transduction domains: enhanced transduction potential in vitro and in vivo. Cancer Research 61, 474–477.

Kabouridis, P.S., 2003. Biological applications of protein transduction technology. Trends in Biotechnology 21, 498–503.

Kaplan, J.M., 2005. Adenovirus-based cancer gene therapy. Current Gene Therapy 5, 595–605.

Kaplan, I.M., Wadia, J.S., Dowdy, S.F., 2005. Cationic TAT peptide transduction domain enters cells by macropinocytosis. Journal of Controlled Release 102, 247–253.

Kawabata, K., Sakurai, F., Koizumi, N., Hayakawa, T., Mizuguchi, H., 2006. Adenovirus vector-mediated gene transfer into stem cells. Molecular Pharmacology 3, 95–103.

Khalil, I.A., Kogure, K., Futaki, S., Harashima, H., 2006. High density of octaarginine stimulates macropinocytosis leading to efficient intracellular trafficking for gene expression. Journal of Biological Chemistry 281, 3544–3551.

Kida, S., Maeda, M., Hojo, K., Eto, Y., Gao, J.Q., Kurachi, S., Mizuguchi, H., Hayakawa, T., Mayumi, T., Nakagawa, S., Kawasaki, K., 2006. Design and synthesis of a Tat-related gene transporter: a tool for carrying the adenovirus vector into cells. Bioorganic & Medicinal Chemistry Letters 16, 743–745.

Kida, S., Maeda, M., Hojo, K., Eto, Y., Nakagawa, S., Kawasaki, K., 2007. Studies on heterobifunctional cross-linking reagents, 6-maleimidohexanoic acid active esters. Chemical and Pharmaceutical Bulletin (Tokyo) 55, 685–687.

Kida, S., Eto, Y., Maeda, M., Yoshioka, Y., Nakagawa, S., Hojo, K., Tsuda, Y., Mayumia, T., Kawasaki, K., 2008. Preparation of a tat-related transporter peptide for carrying the adenovirus vector into cells. Protein Peptide Letters 15, 219–222.

Koizumi, N., Mizuguchi, H., Hosono, T., Ishii-Watabe, A., Uchida, E., Utoguchi, N., Watanabe, Y., Hayakawa, T., 2001. Efficient gene transfer by fiber-mutant adenoviral vectors containing RGD peptide. Biochimica et Biophysica Acta 1568, 13–20.

Koizumi, N., Mizuguchi, H., Utoguchi, N., Watanabe, Y., Hayakawa, T., 2003. Generation of fiber-modified adenovirus vectors containing heterologous peptides in both the HI loop and C terminus of the fiber knob. Journal of Gene Medicine 5, 267–276.

Kuhnel, F., Schulte, B., Wirth, T., Woller, N., Schafers, S., Zender, L., Manns, M., Kubicka, S., 2004. Protein transduction domains fused to virus receptors improve cellular virus uptake and enhance oncolysis by tumor-specific replicating vectors. Journal of Virology 78, 13743–13754.

Kurachi, S., Tashiro, K., Sakurai, F., Sakurai, H., Kawabata, K., Yayama, K., Okamoto, H., Nakagawa, S., Mizuguchi, H., 2007. Fiber-modified adenovirus vectors containing the TAT peptide derived from HIV-1 in the fiber knob have efficient gene transfer activity. Gene Therapy 14, 1160–1165.

Lewin, M., Carlesso, N., Tung, C.H., Tang, X.W., Cory, D., Scadden, D.T., Weissleder, R., 2000. Tat peptide-derivatized magnetic nanoparticles allow in vivo tracking and recovery of progenitor cells. Nature Biotechnology 18, 410–414.

Li, Y., Pong, R.C., Bergelson, J.M., Hall, M.C., Sagalowsky, A.I., Tseng, C.P., Wang, Z., Hsieh, J.T., 1999. Loss of adenoviral receptor expression in human bladder cancer cells: a potential impact on the efficacy of gene therapy. Cancer Research 59, 325–330.

Lu, Y., Zhang, Y., Steiner, M.S., 1998. Efficient identification of recombinant adenoviruses by direct plaque screening. DNA and Cell Biology 17, 643–645.
Maizel Jr., J.V., White, D.O., Scharff, M.D., 1968. The polypeptides of adenovirus. I. Evidence for multiple protein components in the virion and a comparison of types 2, 7A, and 12. Virology 36, 115–125.
Mathis, J.M., Stewart, P.L., Zhu, Z.B., Curiel, D.T., 2006. Advanced generation adenoviral virotherapy agents embody enhanced potency based upon CAR-independent tropism. Clinical Cancer Research 12, 2651–2656.
Meier, O., Boucke, K., Hammer, S.V., Keller, S., Stidwill, R.P., Hemmi, S., Greber, U.F., 2002. Adenovirus triggers macropinocytosis and endosomal leakage together with its clathrin-mediated uptake. Journal of Cell Biology 158, 1119–1131.
Mizuguchi, H., Hayakawa, T., 2004. Targeted adenovirus vectors. Human Gene Therapy 15, 1034–1044.
Mizuguchi, H., Kay, M.A., 1998. Efficient construction of a recombinant adenovirus vector by an improved in vitro ligation method. Human Gene Therapy 9, 2577–2583.
Mizuguchi, H., Kay, M.A., 1999. A simple method for constructing E1- and E1/E4-deleted recombinant adenoviral vectors. Human Gene Therapy 10, 2013–2017.
Mukai, Y., Sugita, T., Yamato, T., Yamanada, N., Shibata, H., Imai, S., Abe, Y., Nagano, K., Nomura, T., Tsutsumi, Y., Kamada, H., Nakagawa, S., Tsunoda, S., 2006. Creation of novel Protein Transduction Domain (PTD) mutants by a phage display-based high-throughput screening system. Biological & Pharmaceutical Bulletin 29, 1570–1574.
Murriel, C.L., Dowdy, S.F., 2006. Influence of protein transduction domains on intracellular delivery of macromolecules. Expert Opinion in Drug Delivery 3, 739–746.
Nakase, I., Niwa, M., Takeuchi, T., Sonomura, K., Kawabata, N., Koike, Y., Takehashi, M., Tanaka, S., Ueda, K., Simpson, J.C., Jones, A.T., Sugiura, Y., Futaki, S., 2004. Cellular uptake of arginine-rich peptides: roles for macropinocytosis and actin rearrangement. Molecular Therapy 10, 1011–1022.
Nakase, I., Tadokoro, A., Kawabata, N., Takeuchi, T., Katoh, H., Hiramoto, K., Negishi, M., Nomizu, M., Sugiura, Y., Futaki, S., 2007. Interaction of arginine-rich peptides with membrane-associated proteoglycans is crucial for induction of actin organization and macropinocytosis. Biochemistry 46, 492–501.
Okada, N., Saito, T., Masunaga, Y., Tsukada, Y., Nakagawa, S., Mizuguchi, H., Mori, K., Okada, Y., Fujita, T., Hayakawa, T., Mayumi, T., Yamamoto, A., 2001a. Efficient antigen gene transduction using Arg-Gly-Asp fiber-mutant adenovirus vectors can potentiate antitumor vaccine efficacy and maturation of murine dendritic cells. Cancer Research 61, 7913–7919.
Okada, N., Tsukada, Y., Nakagawa, S., Mizuguchi, H., Mori, K., Saito, T., Fujita, T., Yamamoto, A., Hayakawa, T., Mayumi, T., 2001b. Efficient gene delivery into dendritic cells by fiber-mutant adenovirus vectors. Biochemical and Biophysical Research Communications 282, 173–179.
Okada, N., Masunaga, Y., Okada, Y., Mizuguchi, H., Iiyama, S., Mori, N., Sasaki, A., Nakagawa, S., Mayumi, T., Hayakawa, T., Fujita, T., Yamamoto, A., 2003a. Dendritic cells transduced with gp100 gene by RGD fiber-mutant adenovirus vectors are highly efficacious in generating anti-B16BL6 melanoma immunity in mice. Gene Therapy 10, 1891–1902.
Okada, Y., Okada, N., Mizuguchi, H., Hayakawa, T., Mayumi, T., Mizuno, N., 2003b. An investigation of adverse effects caused by the injection of high-dose TNFalpha-expressing adenovirus vector into established murine melanoma. Gene Therapy 10, 700–705.
Richard, J.P., Melikov, K., Brooks, H., Prevot, P., Lebleu, B., Chernomordik, L.V., 2005. Cellular uptake of unconjugated TAT peptide involves clathrin-dependent endocytosis and heparan sulfate receptors. Journal of Biological Chemistry 280, 15300–15306.
Roth, J.A., 2006. Adenovirus p53 gene therapy. Expert Opinion on Biological Therapy 6, 55–61.
Rothbard, J.B., Jessop, T.C., Wender, P.A., 2005. Adaptive translocation: the role of hydrogen bonding and membrane potential in the uptake of guanidinium-rich transporters into cells. Advanced Drug Delivery Reviews 57, 495–504.
Schwarze, S.R., Ho, A., Vocero-Akbani, A., Dowdy, S.F., 1999. In vivo protein transduction: delivery of a biologically active protein into the mouse. Science 285, 1569–1572.
Sumida, S.M., Truitt, D.M., Lemckert, A.A., Vogels, R., Custers, J.H., Addo, M.M., Lockman, S., Peter, T., Peyerl, F.W., Kishko, M.G., Jackson, S.S., Gorgone, D.A., Lifton, M.A., Essex, M., Walker, B.D., Goudsmit, J., Havenga, M.J., Barouch, D.H., 2005. Neutralizing antibodies to adenovirus serotype 5 vaccine vectors are directed primarily against the adenovirus hexon protein. Journal of Immunology 174, 7179–7185.
Tomko, R.P., Xu, R., Philipson, L., 1997. HCAR and MCAR: the human and mouse cellular receptors for subgroup C adenoviruses and group B coxsackieviruses. Proceedings of the National Academy of Sciences of the United States of America 94, 3352–3356.
Tunnemann, G., Martin, R.M., Haupt, S., Patsch, C., Edenhofer, F., Cardoso, M.C., 2006. Cargo-dependent mode of uptake and bioavailability of TAT-containing proteins and peptides in living cells. FASEB Journal 20, 1775–1784.
Wadia, J.S., Stan, R.V., Dowdy, S.F., 2004. Transducible TAT-HA fusogenic peptide enhances escape of TAT-fusion proteins after lipid raft macropinocytosis. Natural Medicines 10, 310–315.
Wickham, T.J., Mathias, P., Cheresh, D.A., Nemerow, G.R., 1993. Integrins alpha v beta 3 and alpha v beta 5 promote adenovirus internalization but not virus attachment. Cell 73, 309–319.
Yamamoto, H., Itoh, F., Sakamoto, H., Nakajima, Y., Une, Y., Hinoda, Y., Imai, K., 1997. Association of reduced cell adhesion regulator messenger RNA expression with tumor progression in human hepatocellular carcinoma. International Journal of Cancer 74, 251–254.
Yamashita, M., Ino, A., Kawabata, K., Sakurai, F., Mizuguchi, H., 2007. Expression of coxsackie and adenovirus receptor reduces the lung metastatic potential of murine tumor cells. International Journal of Cancer 121, 1690–1696.